A Numerical Flow Model for North Andros Island, Bahamas: Implications for Circulation and Dolomitization

by
Meredith Westover

A thesis submitted in partial fulfillment of the
requirements for the degree of

Master of Science
Geology

at the
University of Wisconsin - Madison
1994

ABSTRACT

An understanding of fluid circulation patterns and the mechanisms that drive fluid flow in carbonate banks is necessary to understand the extent, distribution and type of diagenetic alteration we observe in the ancient rock record. In this study, a density dependent groundwater flow model for North Andros Island and the Great Bahama Bank is developed to quantify flow induced by elevation potential and thermal convection. Special attention is paid to the dolomite problem, both as an example of how research on diagenesis has led to the conceptualization of fluid flow in carbonate banks, and as a tool for the interpretation of modeling results.

Groundwater flow simulations in absence of heat or solute transport were run to test the models sensitivity to elevation potential across Andros Island, bank heterogeneity, and anisotropy. A net eastward flow under Andros Island as hypothesized by Whitaker and Smart (1993) could only be generated by high horizontal to vertical anisotropy ratios, or in the case where the elevation potential across the island was greater than the head within the island.

Bank heterogeneity had the effect of channeling flow into high conductivity units. This effect was enhanced when the relative differences in permeability between zones was increased by orders of magnitude. Changes made to the overall permeability of the system were reflected by similar changes in velocity.

Based on groundwater flow results, some comments may be made on diagenesis in general and on dolomitization in particular. Highest fluid velocities found directly beneath Andros Island and in the high permeability Holocene bank top deposits could be sites of early, pervasive cementation (high mass fluxes), or in the case of mixing zone flow, intense dissolution.

Areas of low groundwater flow such as groundwater divides may be zones in which primary mineralogy, porosity and fabrics are preserved. The location of the groundwater divide is highly dependent on bank heterogeneity and anisotropy.

Mass fluxes calculated from the velocity output allows an estimate of the time required to dolomitize the bank. Estimates of magnesium mass fluxes from this study are comparable to those of Kaufman (1994). Based on these data, 100% dolomitization requires more than one million years.

Heat transport simulations were largely unsuccessful, due to numerical problems and time constraints. No meaningful output could be generated even with reduced grid spacing and short time steps.

ACKNOWLEDGEMENTS

I would like to thank my committee, Jean Bahr, Mary Anderson, and Toni Simo for advising and assisting me on this project. My major adviser, Jean Bahr deserves credit for accomplishing the near impossible--turning a complete computer phobe like myself into a computer modeller in just two years. Jean, I admire your patience and persistence. I am infinitely grateful to Bill Arnold, who provided FORTRAN codes I could butcher, tips on deciphering HST3D, and instruction on using Artesia, our pet Silicon Graphics workstation. I am also thankful to Martha Gerdes and Ben Abernathy for their help with FORTRAN when my butchering attempts failed.

Thank you also to Gregor Eberli, Peter Swart, and Leslie Melim at the University of Miami, Rosenstiel School of Marine and Atmospheric Science (RSMAS), and Philip Weech at the Water and Sewerage Corporation, Nassau, Bahamas, who provided contacts and a wealth of information about the Bahamas...and of course to the Department of Energy and the Ocean Drilling Program for furnishing me with enough money to eat while I wrote this thesis.

This thesis is dedicated not only those of you who taught me the moral of grad school, "if at first you do succeed, be very, very suspicious", but to those who helped me deal with the realization as well. I don't think that I would have survived this ordeal without the support of my friends and family, many of whom have already experienced the trials, tribulations, and finally the overwhelming joy of completing a thesis. I am grateful to my parents for their inexhaustible support, for encouraging me to continue my education, and for reminding me that I have a place to stay when I graduate, unemployed. I am deeply indebted to Mary Ann Kelly and Teufelin Peare for keeping me (relatively) sane during my two-plus

years in Madison. Tuff, I have two words for you--Raptor Bites. Mary Ann, I will never forget our enlightening conversations on such topics as gray hairs, fish nostrils, and pig urine. Even if no one else understands, I think *I* may have learned a little bit about life. And to Eric Oelkers...what can I say? Thank you for just being you. Those of you back home are not forgotten by any means. Lence, Nedley, and Cathie--the never ending flow of gummi bears and random bizarre tidbits through the mail always made me look forward to coming home at the end of the day.

Wait, I'm not *quite* finished. I have one more very special thank you: To the thug in Baltimore who ever so lovingly removed thesis notes and papers from my possession in March--thank you for giving me the opportunity to reinforce my knowledge of the subject by rereading dozens of papers. Thank you so much.

: no space left on device

TABLE OF CONTENTS

Chapter 1

INTRODUCTION

- INTRODUCTION -

The purpose of this thesis is to develop a density dependent ground water flow model for North Andros Island, Bahamas and the Great Bahama Bank. Such a model can be used not only to predict flow patterns and quantify flow in isolated carbonate platforms, but also to provide insight into the kinds of mechanisms responsible for driving fluid flow and problems of diagenesis.

Fluid circulation patterns in isolated carbonate platforms control the extent, distribution, and type of diagenetic alteration that is observed in the rock record. Diagenetic alteration of these platforms results in features of potential economic importance, especially the formation of significant secondary porosity or diagenetic seals. Carbonate geochemistry is very complex, making diagenetic alteration in carbonate environments all the more difficult to understand. Slight differences in the composition of the substrate, water chemistry, or fluid flow rates can mean the difference between extensive dissolution or extensive precipitation. Large porosity differences between recent (40-70% porosity) and ancient carbonates (often less than 5% porosity) suggest that vast quantities of carbonate material must be added to the rock by way of the circulating fluids (Bathurst, 1975). In addition, most ancient carbonates have been at least partially dolomitized, a reaction that requires even more stringent constraints on water chemistry. In the next section, the problem of forming massive dolomite will be discussed as an example of how

diagenetic research has led to the conceptualization of fluid flow in carbonate platforms.

The goal of the research presented in this thesis is to quantify flow induced by such mechanisms as elevation potential and thermal convection in a heterogeneous and anisotropic carbonate platform. Specifically, I will focus on the model's sensitivity to each driving mechanism and to bank heterogeneity. Fluid velocity output from this model will be available to calculate magnesium fluxes within the bank, allowing for discussion of the model's implications for dolomitization.

- THE DOLOMITE PROBLEM -

Dolomite, in its purest stoichiometric and well ordered form, is simply $CaMg(CO_3)_3$, with CO_3 anion planes alternating with Ca and Mg cation planes (Land, 1983). Although there is a strong thermodynamic drive to precipitate dolomite directly from normal seawater (seawater is many times supersaturated with respect to this mineral), no one has observed direct precipitation in modern marine environments (Badiozamani, 1973 and Land, 1983). In fact, it has not been possible to precipitate stoichiometric dolomite in a laboratory at surface conditions (Illing et al., 1965 and Hardie, 1987). In modern marine environments, the type of dolomite that forms is a small amount of weakly ordered, calcian dolomite $Ca(Ca_{.16}Mg_{.84})(CO_3)_2$ (e.g. Deffeyes et al., 1965; Hardie, 1977; Gebelein, et al., 1980; and Stoessell et al., 1989). Looking at the ancient rock record, however, we see large quantities of massive dolomite. How can we explain this discrepancy? Most researchers believe that massive dolomite is the result of post-depositional diagenetic alteration of limestone or "proto-dolomite" (metastable weakly-ordered calcian dolomites). In this scenario, it is necessary to have a mechanism or process that 1) supplies and distributes magnesium and 2) provides a favorable

geochemical environment for the precipitation of dolomite (Adams and Rhodes, 1960; Deffeyes et al., 1965; and Aharon et al., 1987). Since little is known about the chemistry of dolomitization due to the difficulties in precipitating the mineral in laboratory settings, a "favorable geochemical environment" is not very well defined. With these requirements in mind, many conceptual models of dolomitization have been developed.

Massive dolomitization is most likely a precipitation/dissolution reaction governed by kinetics (Hardie, 1987; and Land, 1983). While dolomite does not precipitate readily in a lab at surface conditions, it will precipitate in a matter of days at 100°C (Baron, 1960 (as cited in Hardie, 1987); and Gaines, 1980). Experimental studies have described some kinetic limitations on the precipitation of dolomite at 100°C. For instance, Gaines (1980) found that the reaction was fastest when "seeded" with proto-dolomite and that the reaction rate could be increased by stripping water from Mg^{++} ions, or by increasing the Mg/Ca ratio (up to about 5). In addition, Gaines found salinity to be a significant control on the reaction rate. Baker and Kastner (1981) found that $SO_4^{=}$ ions have a rate-inhibiting effect, due to lattice poisoning. These experimental studies have led researchers to develop "special waters" approaches to dolomitization. That is, if we can alter the temperature, add catalysts, reduce inhibitors (Hardie, 1987), it is possible to create a fluid that is capable of dolomitizing just about anything. Two principle models have come out of this "special waters" era: the Hypersaline Brine model (including supratidal dolomite) and the Mixing Zone ("Dorag") model (Boggs, 1987; and Hardie,1987). The hypersaline brine model requires a restricted environment like that of an evaporitic lagoon (Adams and Rhodes, 1960) or sabkha (McKenzie, 1980), where seawater can be gradually evaporated and concentrated. As the brine becomes more concentrated, aragonite and gypsum precipitate, driving

up the Mg/Ca ratio and reducing the $SO_4^{=}$ concentration. The remaining fluid is thought to be an ideal dolomitizing fluid (Figures 1 and 2). These and other hypersaline dolomites are most often associated with evaporite deposits (e.g. gypsum).

Looking again at the ancient rock record, it becomes clear that many dolomites are not in any way associated with evaporites or evaporitic settings. To explain these dolomites, another model must be presented. The mixing zone model is based on the premise that, due to ionic strength effects, dolomite saturation increases with increasing seawater concentrations from 5% to 30% seawater (Figure 3). Within this range, the waters will be supersaturated with respect to dolomite, while undersaturated with respect to calcite (calcite should dissolve while dolomite is precipitated). Because of the ionic strength effects of mixing waters, the Mg/Ca ratio does not need to be higher than 1 in order to create a dolomitizing fluid (Badiozamani, 1973).

In order to justify the use of "special waters" to explain the formation of massive dolomites, it should be possible to identify the chemistry associated with these waters in the rock record. In other words, one would like to look at the isotope and trace element chemistry of any given dolomite and be able to determine the fluid chemistry of the environment where it formed (e.g. Ward and Halley, 1985 and Aharon et al., 1987). Unfortunately, there are many problems with the methods being used in diagenetic studies. For example, the isotopic composition of the dolomite depends not only on the dolomitizing fluid, but on the initial rock as well, and often the samples analyzed represent a mixture of both. Trace element chemistry complicates matters further. Trace element partitioning into the dolomite phase depends on many kinetic factors, including the ratios of

elements in the aqueous phase, temperature, pressure, and crystal growth rate, to name just a few (Land, 1983; Hardie, 1987).

Other problems with "special waters" interpretations are specific to individual models. The sabkha model for hypersaline dolomite, for example, was developed to explain the observed brine stratigraphy in evaporitic settings. If it is assumed that the system consists of two sources of water, a continental source and a marine source, it is possible to exactly reproduce the brine stratigraphy without ever requiring dolomitization to occur (Hardie, 1987). One point in favor of the sabkha model is that modern analogs do exist, like the Abu Dhabi sabkha in the Persian Gulf. The mixing zone model has a rather larger problem. Despite the thousands of kilometers of modern carbonate coastline and platforms with well developed fresh water lenses, no significant modern mixing zone dolomite is found (Stoessell et al., 1989). These problems have forced researchers to move away from the "special waters" approach, switching the emphasis to the influence of temperature and time on dolomitization, and to mass transfer processes--e.g. how do you supply and distribute magnesium throughout the bank over a long period of time?

Time and mass transfer processes are important aspects in any diagenetic study, not just to the problem of forming massive dolomite. The creation of significant amounts of secondary porosity or deposition of cement also requires large fluid fluxes.

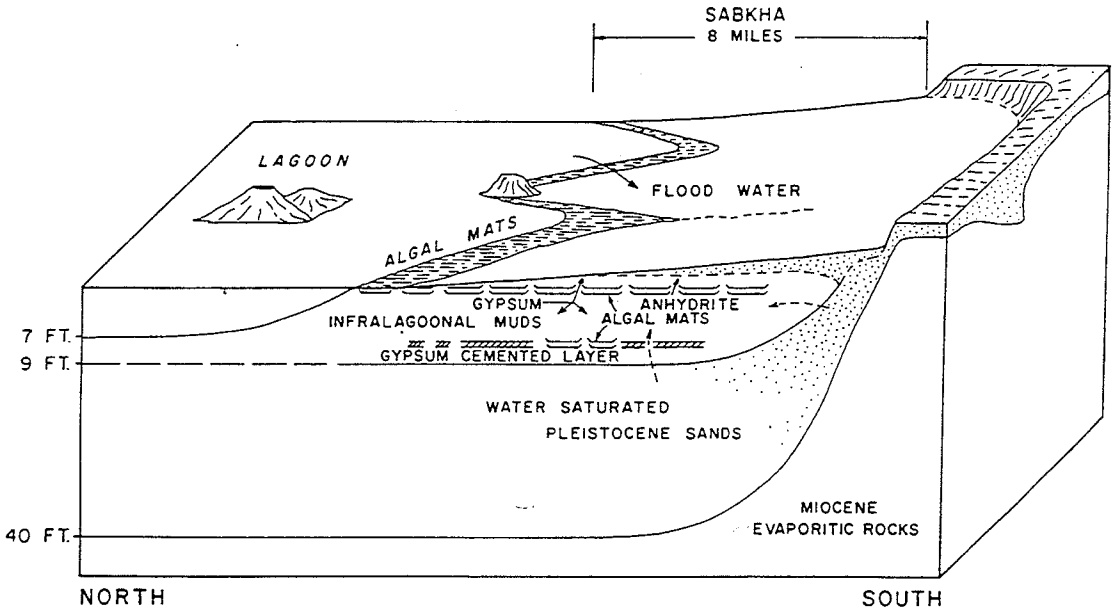

Figure 1. Schematic diagram of the Abu Dhabi sabkha in the Persian Gulf (from Butler, 1969).

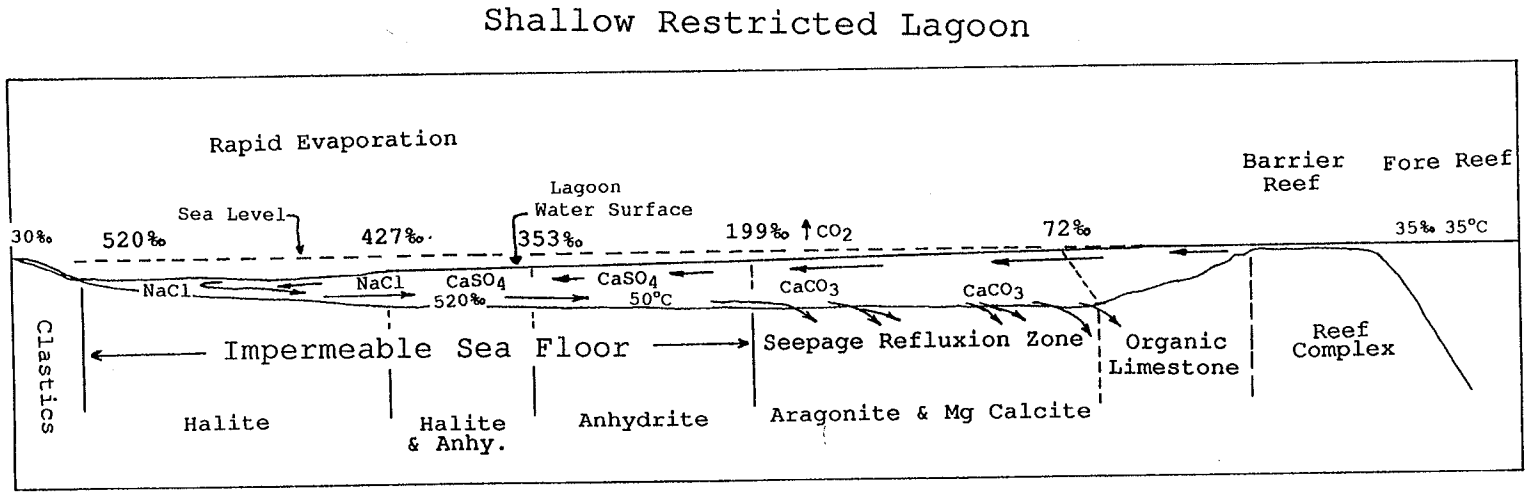

Figure 2. Schematic diagram of brine stratigraphy in an evaporite lagoon (modified from Adams and Rhodes, 1960)

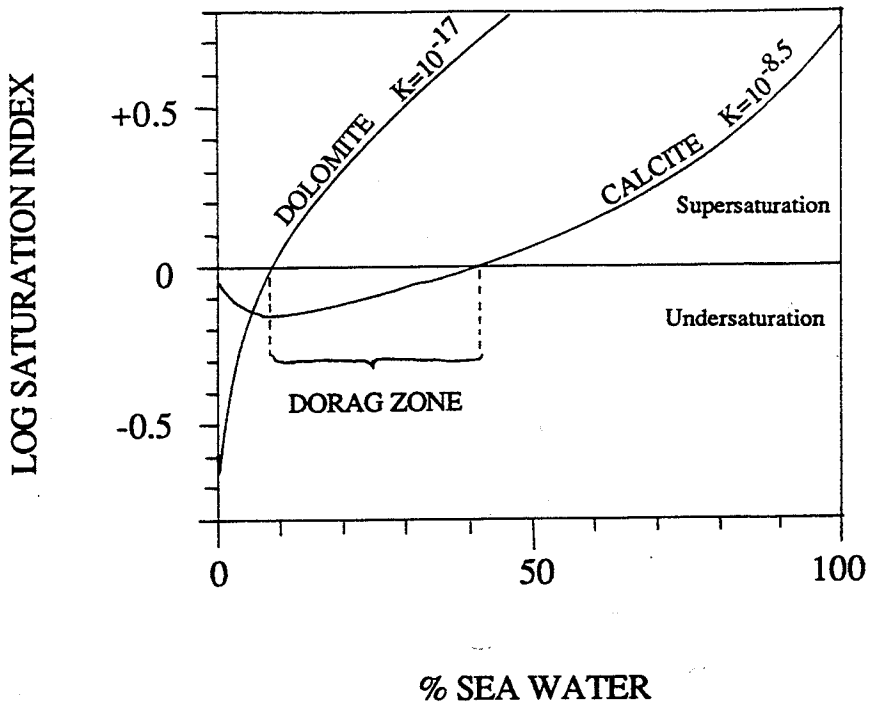

Figure 3: Dolomite and calcite saturation state in seawater/meteoric water mixtures at 25°C (modified from Hardie, 1987).

- CONCEPTUAL MODELS OF FLUID FLOW IN CARBONATE BANKS -

This new approach to the dolomite problem has prompted the development of many new conceptual models within the last decade. Simms (1984) and Whitaker and Smart (1993) present several mechanisms to drive fluid flow in carbonate banks. The first of these mechanisms is reflux (as proposed by Adams and Rhodes, 1960), where seawater becomes concentrated by evaporation, the resulting brine becomes more dense than the underlying fluids, and it sinks through the bank (Figure 4a). In addition to the flow induced by such circulation, the slightly elevated salinities and elevated Mg/Ca ratio of these waters make these fluids more favorable dolomitizing fluids than normal marine waters. The salinity of bank waters on the western Great Bahama bank is only slightly higher than normal marine waters--36‰ to 46‰ (42‰ to 45‰ over large portions of the bank; Morse et al.,1984 and Simms, 1984). Based on stability theory, Simms (1984) calculated a Rayleigh number (Ra) of 80 for water of 42‰ salinity. Flow should proceed for unstable conditions, where $Ra > 0$ (upward increase in density). Simms demonstrated in a sandbox model that a Rayleigh number of 80 was sufficient to generate flow to great depth. It is estimated that reflux, without interference by tides, etc., could generate flow within the Bahama bank to depths up to 1000 feet (Simms, 1984).

Buoyant circulation in the mixing zone operates only on a small scale, but is an important driving mechanism as well (Figure 4b). Freshwater overlying denser seawater within emergent portions of the bank flows seaward, driven by freshwater head within the island. At the freshwater/saltwater interface, seawater mixes with the freshwater and becomes entrained in the seaward flow. The salt water lost in this process is then replaced at depth from the bank margin. Although small in scale, repeated rises and falls in sea level will move the mixing zone around

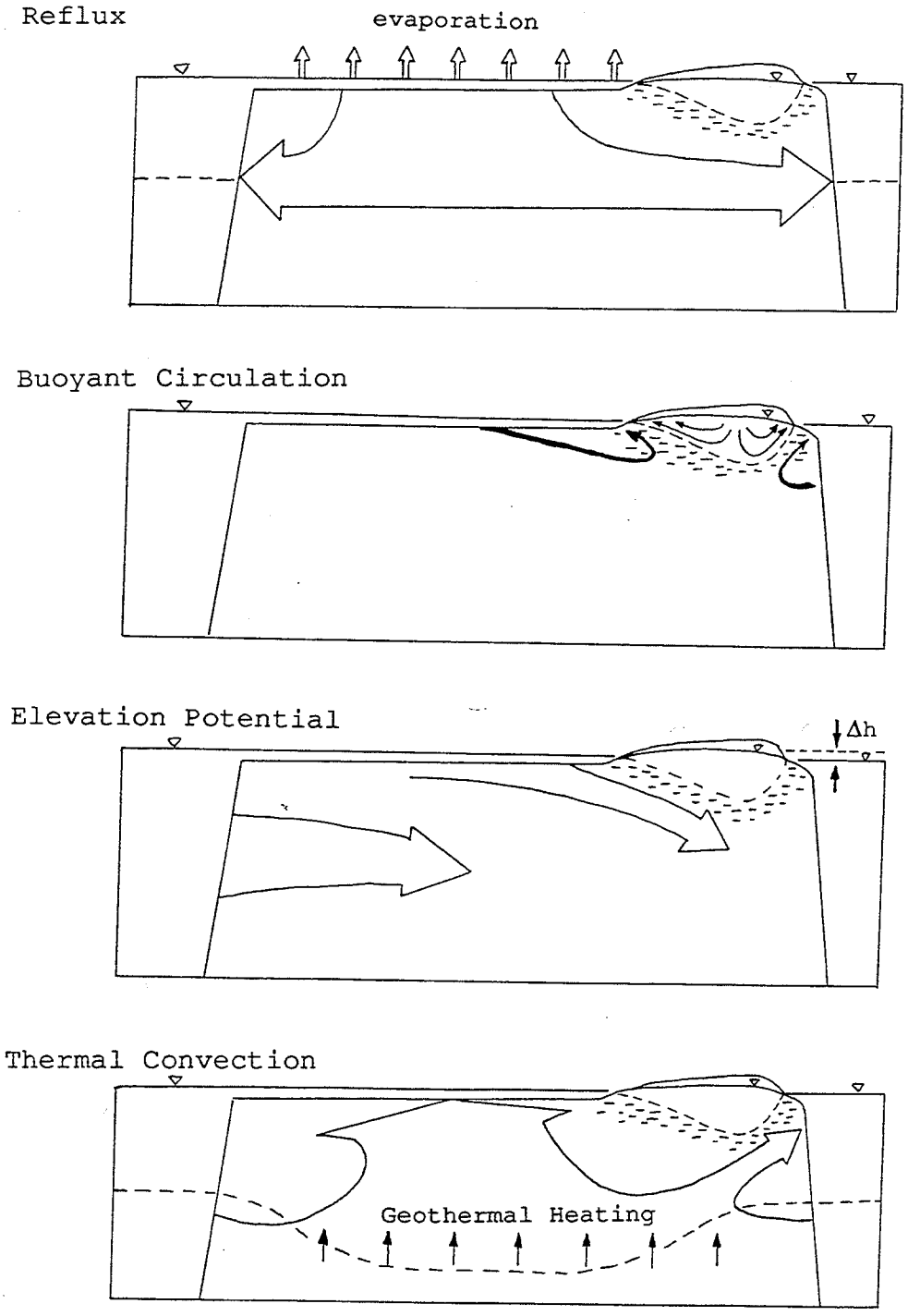

Figure 4. Mechanisms responsible for driving fluid flow in carbonate banks (modified from Whitaker and Smart, 1990): a) density driven reflux of dense bank brines, b) buoyant circulation in the mixing zone, c) elevation potential across North Andros Island, d) thermal (Kohout) convection.

(provided that enough time passes for the development of a freshwater lens), and could account for massive dolomitization (Badiozamani, 1973).

Elevation potential is simply the flow of water from high head (or flow potential) to low head (Figure 4c). In an isolated carbonate platform like the Bahamas, this elevation potential across the island could be generated on three time scales: 1) diurnal tidal fluctuations on the order of 20 cm or so, 2) wind and wave set up on the western bank (days to months or longer), and 3) ocean currents (thousands to millions of years). In the context of dolomitization, probably only the ocean currents are operational over long enough time periods to create a suitable flow system.

Thermal convection was proposed by Kohout (1967) to explain negative geothermal gradients in the Floridan platform (Figure 4d). This process involves flow driven by a slight density gradient between warm pore fluids and the surrounding seawater. Pore waters in the bank are heated by geothermal energy, become less dense, rise, and are replaced at depth by colder, denser ocean waters. The scale of this circulation system can be enhanced by the presence of cavernous porosity, which has been observed to great depths in Florida and the Bahamas (Kohout, 1967; Spencer, 1967).

Combining all of these driving mechanisms, Whitaker and Smart (1993) have proposed two resulting flow systems (Figure 5). The first of these is basically a large convection cell where warm waters rise within the bank, mix with elevated salinity (dense) bank waters, and flow laterally to the platform margins. In the second model, there is a net eastward flow of two near normal marine waters underneath Andros Island--cold ocean water derived from the Straits of Florida, and slightly elevated salinity water from bank reflux. Thermal convection plays little, if any, role in the development of this circulation system. This second model

accounts for the low temperatures and elevated salinities found in inland blue holes on North Andros Island (Whitaker and Smart, 1993). It is necessary to keep in mind that these conceptual models are completely theoretical. Bank heterogeneity is not accounted for in any way, and these processes may very well act in opposition to one another (e.g. temperature and salinity (evaporative reflux) on density; Whitaker and Smart, 1993). The development of these conceptual models is an important step toward understanding the mechanisms that drive fluid flow in carbonate platforms. The next step is to try to quantify fluid flow through the use of numerical models.

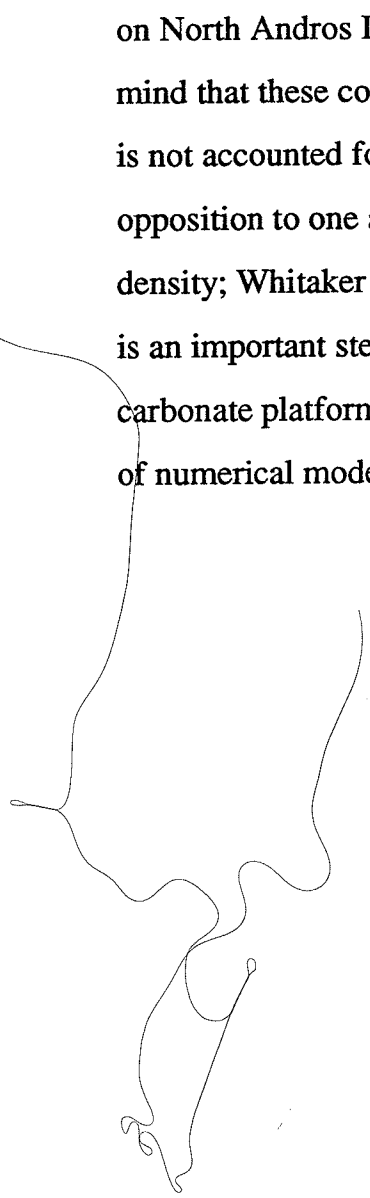

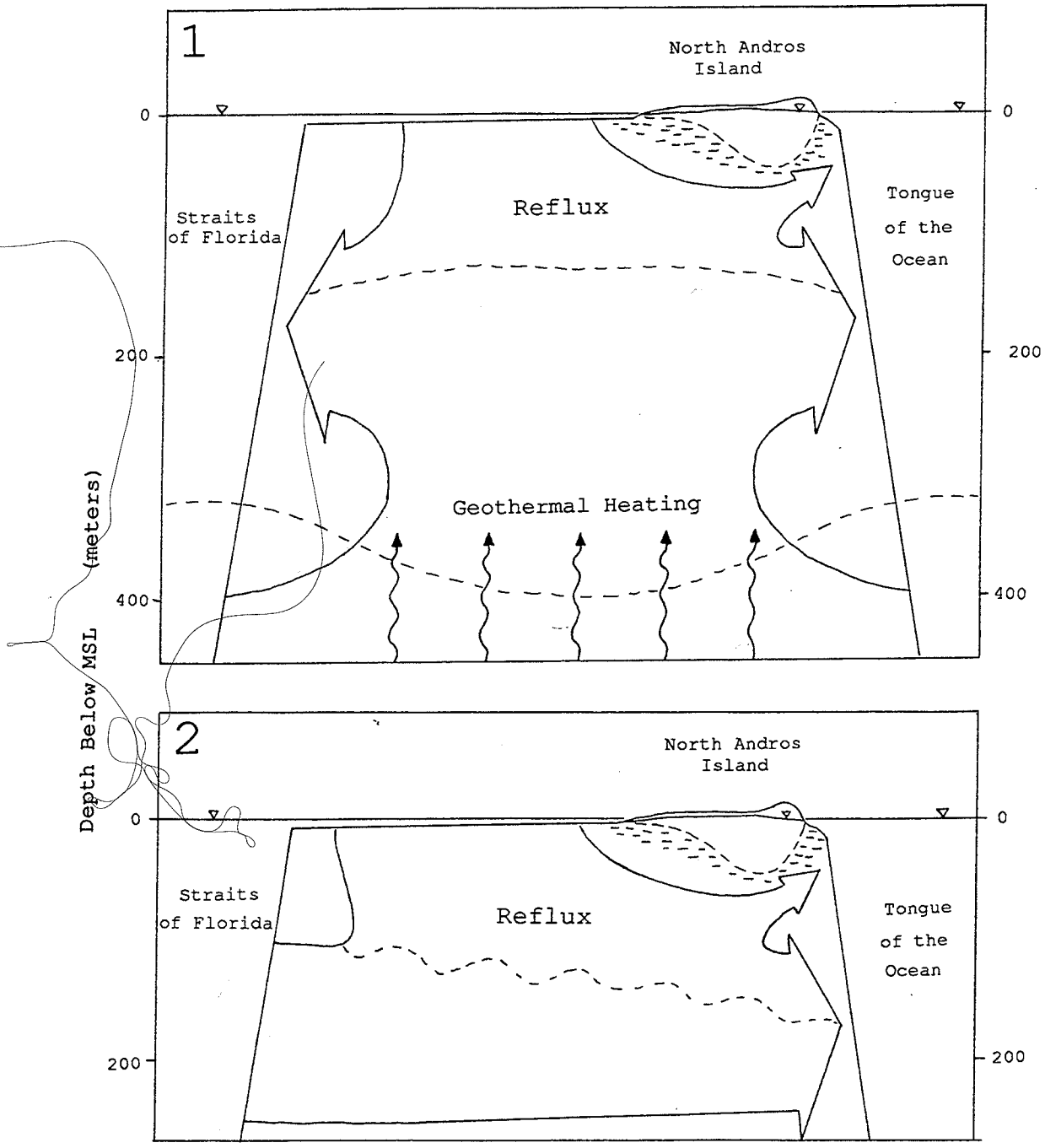

Figure 5. Conceptual models of fluid circulation in carbonate banks (modified from Whitaker and Smart, 1990).

Chapter 2

QUANTITATIVE ANALYSIS OF FLUID FLOW IN CARBONATE BANKS:

- HISTORY -

Reilly and Goodman (1985) provide an overview of the history of quantitative analysis of freshwater-saltwater relationships. Early quantitative analysis began with the description of a sharp interface between the two fluids. Ghyben (1888) and Herzberg (1901) described the relationship of fresh and salt waters under hydrostatic conditions based on the density differences between the fluids. Muskat (1937) and Hubbert (1940) determined the position of the interface using the principle of continuity of pressure across the interface, which in effect separated the fresh and salt water flow fields, allowing for fluids in motion. Growing concern over water supply problems required the consideration of not only the position of the interface, but the overall water quality. A sharp interface model was no longer sufficient to represent the fluid relationships due to mixing of waters. Cooper (1959) presented a hypothesis to explain the mixing of fresh and salt waters and noted the resulting circulation when saltwater becomes entrained in the seaward flow of freshwater. These effects of density dependent flow and dispersion in the transition zone on seawater intrusion required not only ground water flow to be accounted for, but solute transport as well. Henry (1959) quantified these effects through the use of the advection-dispersion equation. This was followed by an analytical solution in 1964 (Henry, 1964 as cited in Griggs and Peterson, 1993). Better understanding of the causes of dispersion and the

importance of the location and thickness of the transition zone has led to greater effort toward aquifer characterization.

- NUMERICAL MODELING -

Regional scale aquifers, when not under the influence of stresses like pumping or tides, often have relatively narrow transition zones, but significant numerical problems exist in representing these zones. Dispersion parameters are not well known and are difficult to estimate, and simulation problems include spatial instabilities in the numerical concentration solution, insufficient discretization to capture a narrow front, numerical errors in calculating fluid velocities, and inaccurate representation of density driven flow (Voss and Souza, 1987). These problems can result in large numerical errors (numerical dispersion), thus preventing the accurate representation of narrow transition zones.

Water supply problems on an atoll island scale have called attention to the problems accounting for numerical dispersion and its effects on the size of the transition zone. Ghassemi et al. (1990) applied the density dependent flow model SUTRA (Saturated-Unsaturated TRAnsport, Voss, 1984) to model seawater intrusion on Nauru Island in the Central Pacific Ocean. Nauru Island is a raised carbonate atoll underlain by a thin (4.7m avg.) freshwater lens and a very thick transition zone. This study and a subsequent one using HST3D (Heat and Solute Transport in Three Dimensions, Kipp, 1987) in addition to SUTRA (Ghassemi et al., 1993), showed that the salinity distribution is strongly influenced by aquifer heterogeneity--the thick transition zone was most likely due to the high permeability of the karstified limestone. Griggs and Peterson (1993), also realizing the necessity of aquifer characterization in modeling narrow transition zones, incorporated some aquifer heterogeneity into their model. Also using the model

SUTRA, they tested the model's sensitivity to various aquifer parameters and found that the thickness of the transition zone was most sensitive to transverse dispersivity. This supports the conclusions of Voss and Souza (1987) that the narrowest possible transition zone is given when transverse dispersivity is equal to zero.

A somewhat different approach to modeling was taken by Kaufman (1994). Instead of looking at a case study and focusing on water supply, he looked at fluid driving mechanisms in a hypothetical homogeneous, isotropic, steep sided carbonate platform. Kaufman successfully reproduced flow systems driven by topography, brine reflux and thermal convection. All of these mechanisms were found to transport magnesium efficiently within the bank, but must be operational over thousands to millions of years to produce massive dolomite.

Like the work of Kaufman (1994), the research presented in this thesis was designed to look at fluid flow induced by specific mechanisms in a carbonate platform. By modeling a natural system, however, the effects of bank heterogeneity and anisotropy can also be described.

Chapter 3

BAHAMAS GEOGRAPHY AND GEOLOGY

- REGIONAL SETTING -

The Great Bahama Bank is a steep-walled isolated carbonate platform located approximately 100 kilometers east of the southeast coast of Florida, separated from the Florida Plateau by the Straits of Florida (Figure 6). The Gulf Stream current flows through the Straits, piling water on the western bank and creating an elevation differential between sea level on the west bank and the Tongue of the Ocean (TOTO). The magnitude of this head difference is unknown, but could be quite large--the sea level difference between Miami and Bimini Bank is about 66 centimeters (Whitaker and Smart, 1993). The Tongue of the Ocean forms a deep inlet into the bank on the eastern side of North Andros Island.

North Andros Island is the largest Pleistocene island in the Bahamas archipelago and consists of a series of northwest to southeast trending facies belts. Pleistocene dunes up to tens of meters elevation form the eastern island margin, with low Pleistocene oolite shoals and Holocene fresh water marshes to the west. Holocene tidal flats make up approximately half of the island on the western margin where the gently sloping Pleistocene bedrock surface dips below sea level (Gebelein et al., 1980). Beyond the tidal flats, a shallow bank extends approximately 100 kilometers to the west, forming a restricted shallow water environment. Here bankwaters often reside up to a year, and range in salinity from 36‰ to 42‰ (Morse et al., 1984; and Simms, 1984).

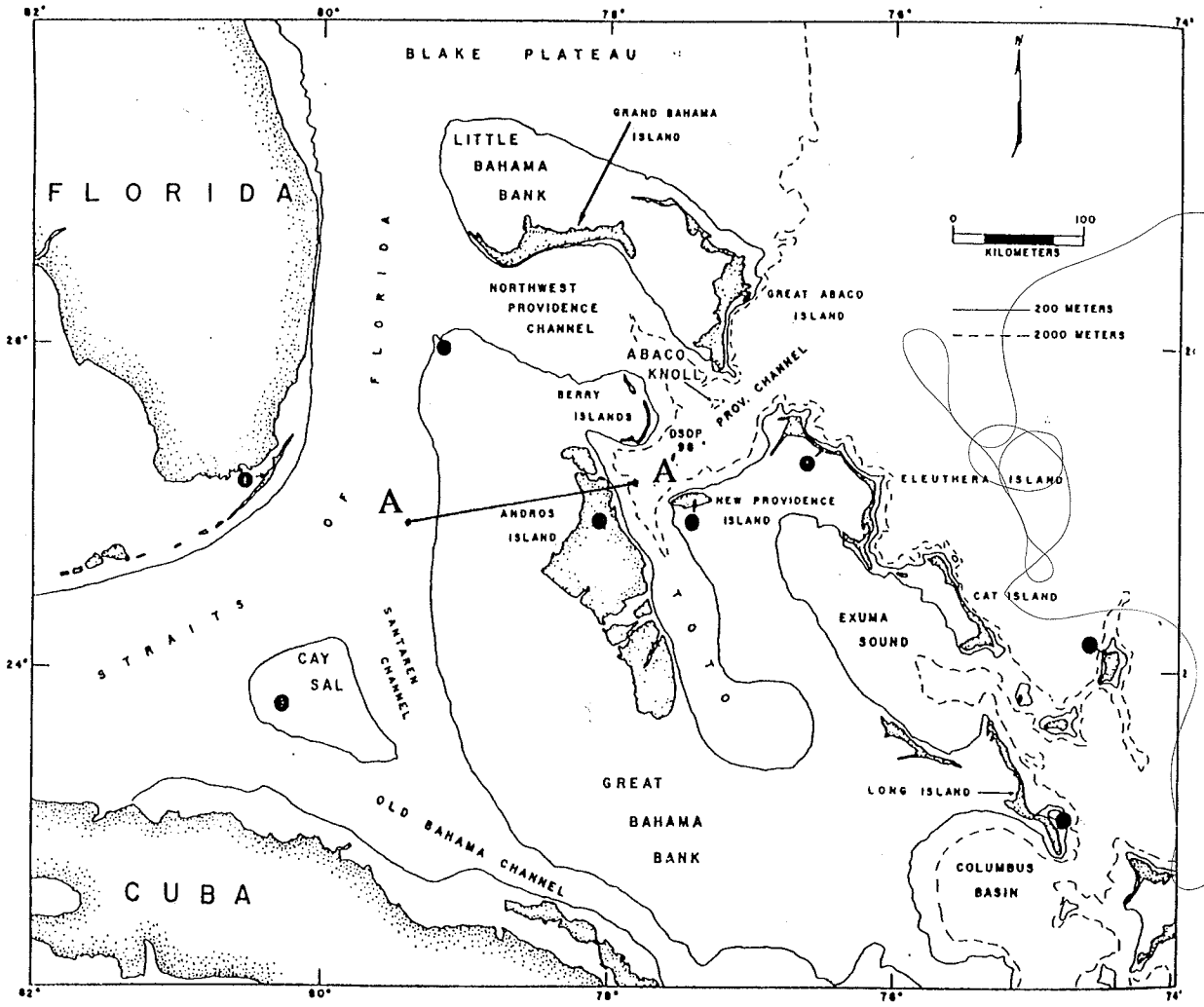

Figure 6. Index map of the northwestern Bahama Platform (From Mullins and Lynts, 1977).

Great Bahama Bank stratigraphy is defined by high resolution seismic lines in conjunction with two cores from the Bahamas Drilling Program (Eberli and Ginsburg, 1987 and 1989; cores CLINO and UNDA, Figure 7 and Figure 8). Core UNDA encounters three successions of reefal/shallow water (highstand) deposits alternating with two deeper water sequences, representing periods of margin backstepping during rapid sea level rise. Core CLINO shows only a single reefal unit overlying thick slope (deep water) deposits (Eberli et al., 1993). From this information, a generalized cross section of the Great Bahama Bank can be constructed (Figure 9).

Based on examination of the cores CLINO and UNDA and the seismic profiles, the bank can be divided into five sections, and three different hydrogeologic units. The first of these zones is made up of the Holocene deposits that drape the uppermost bank. The sediments consist of broken coral fragments and coarse skeletal sands and exhibit vuggy porosity of both primary and secondary origin. As a whole, this zone has very high porosity and permeability, and is probably more or less isotropic. The remainder of the bank can be further subdivided into Straits deposits and Bank deposits. Cores CLINO and UNDA penetrate only the uppermost portion of the Straits of Florida deposits, and aquifer parameters are determined from the core logs. Permeability of these deposits is highly variable, ranging from the order of 0.5 to 5000 millidarcies (5×10^{-16} m^2 to 5×10^{-12} m^2). The permeability varies greatly in a vertical direction, alternating between vuggy porosity and extremely tightly cemented sections. Neutron porosities ranged from about 20% to 70%. It is assumed that the Straits of Florida and Straits of Andros deposits behave essentially the same hydraulically, due to their similar depositional setting. Bimini and Andros Bank deposits are treated separately. Little is known about these deposits as seismic waves failed to

penetrate them and few core data exist (Superior Deep Test Well, Spencer, 1967; Goodell and Garman, 1969). Based on similar ancient carbonate assemblages, I have assumed that these units will have similar stratigraphy to the Straits deposits, but may have slightly lower hydraulic conductivity, say by one order of magnitude (Eberli, pers. comm., 1994). The Bahamas Deep Test Well shows evidence for cavernous porosity to great depths (Spencer, 1967), so this conductivity could be quite high.

- CLIMATE -

North Andros Island lies in a subtropical zone in the east, northeast trade wind belt. Yearly rainfall averages 110 to 120 cm/yr, most of which falls between May and October. Two types of storms dominate: winter storms are lingering northwesterly fronts (several days in duration), and occasional hurricanes strike during the late summer and early fall. Mean temperatures range from about 28 °C in August and September to 22°C in December and January. Open water evaporation nets about 150 cm/yr (all climatic data from Gebelein, 1980).

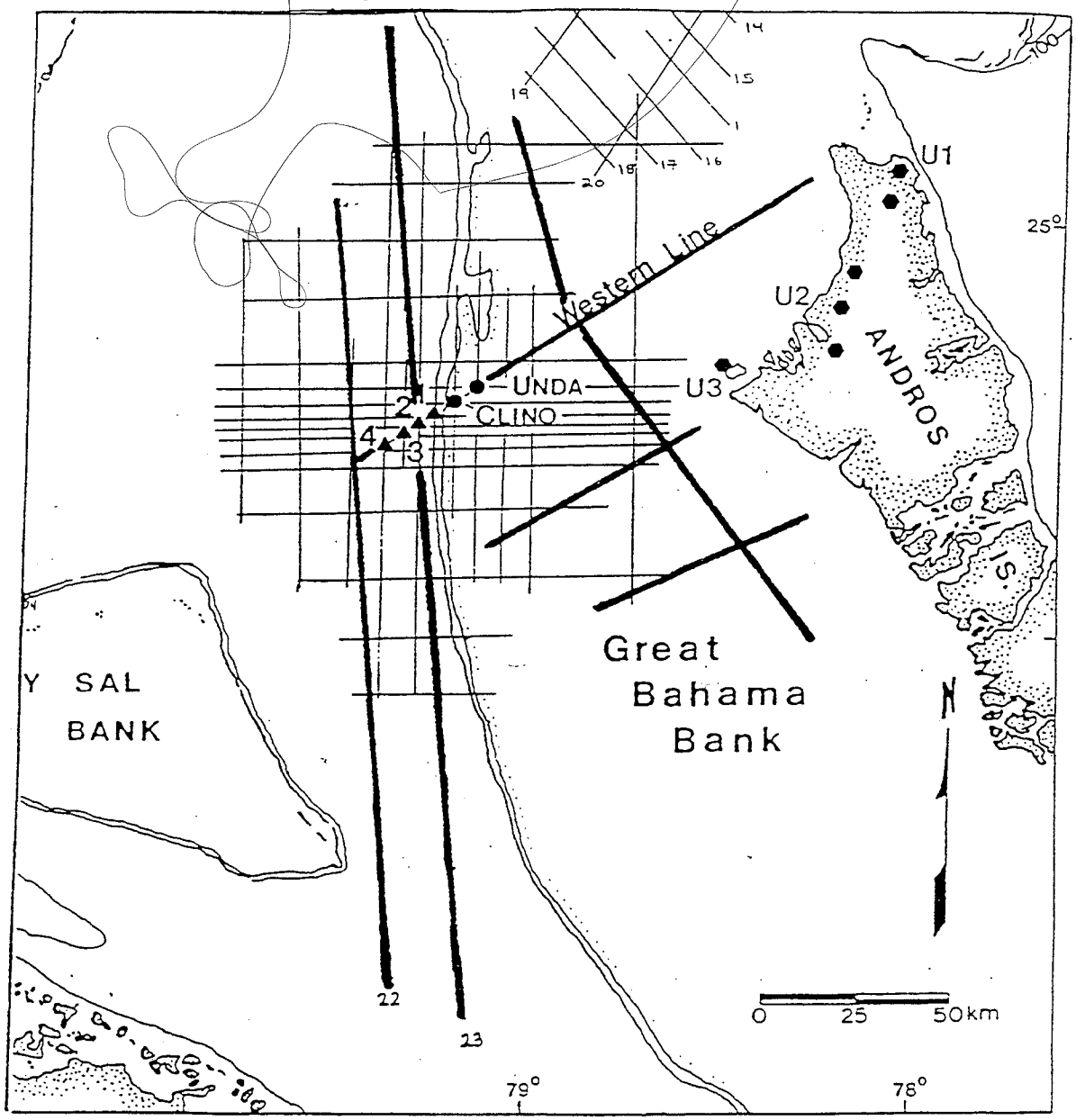

Figure 7. Locations of Bahamas Drilling Program core holes CLINO and UNDA, and high resolution seismic lines (from Eberli et al., 1992).

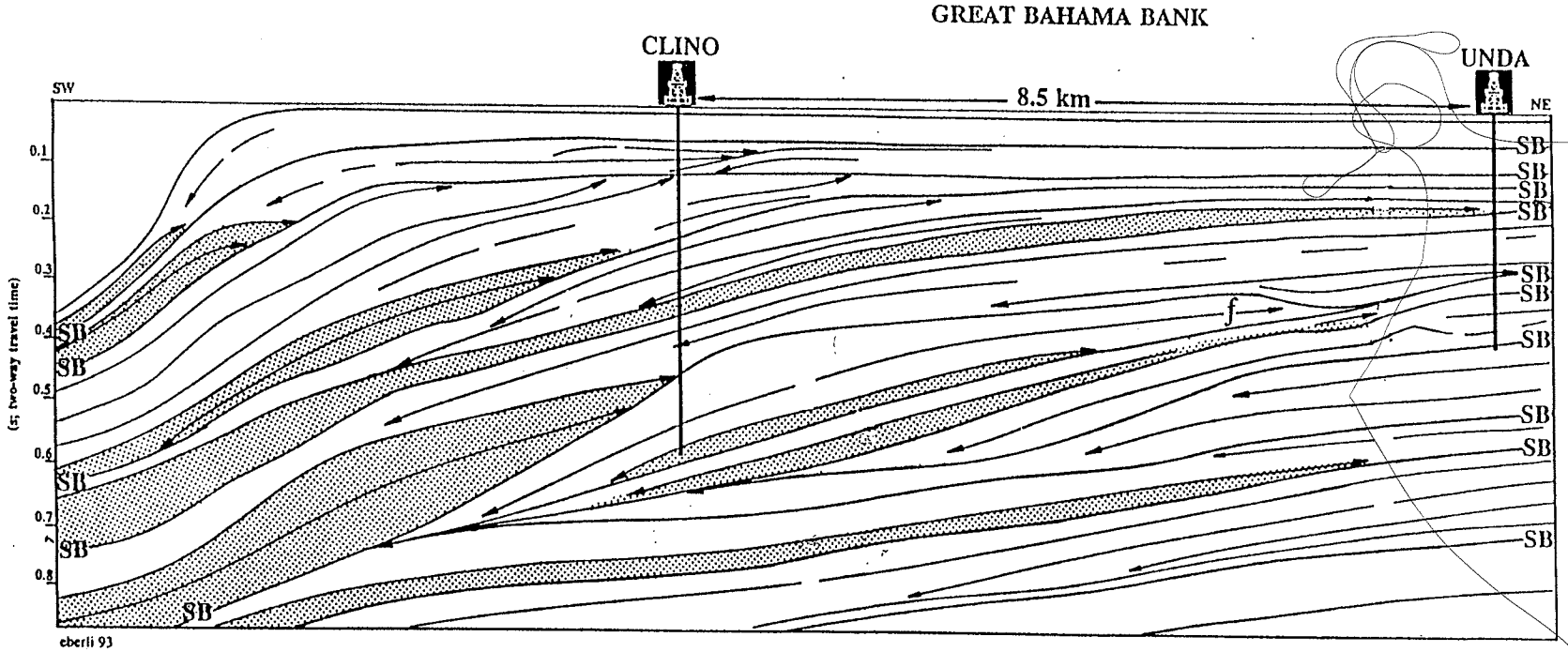

Figure 8. Western Great Bahama Bank stratigraphy as defined by cores CLINO and UNDA and seismic profiles (from Eberli et al., 1992).

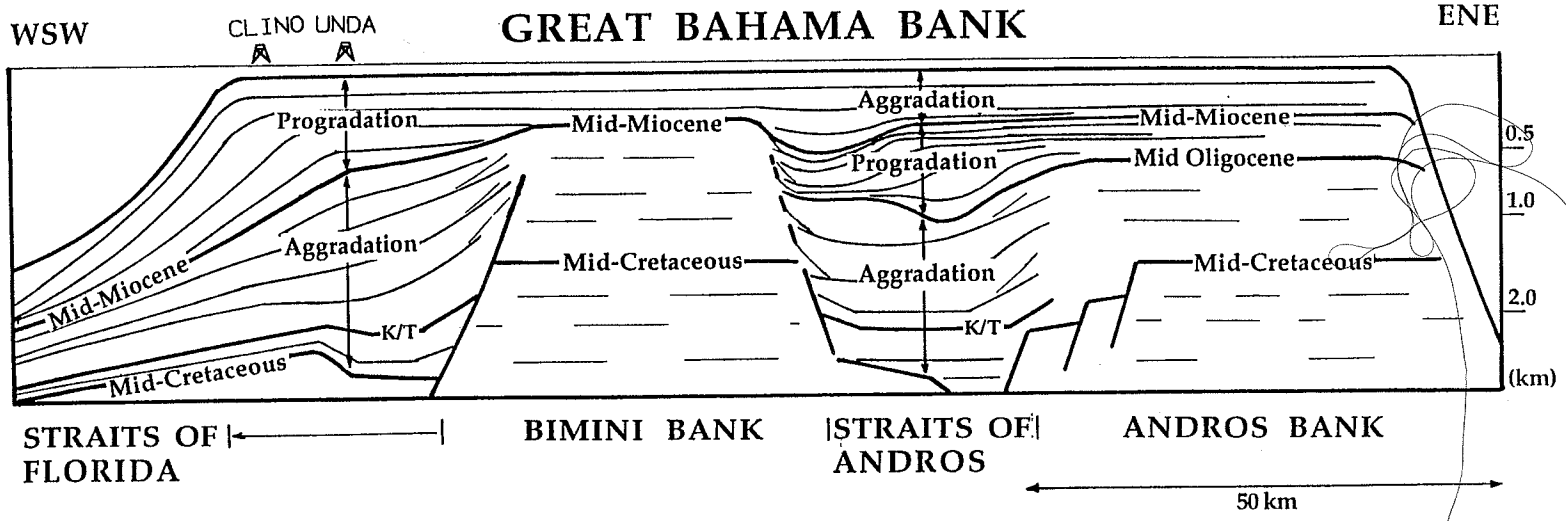

Figure 9. Stratigraphy of the Great Bahama Bank from seismic data (from Eberli, pers. comm., 1994). Approximate locations of core holes CLINO and UNDA are shown.

Chapter 4

A NUMERICAL FLOW MODEL FOR NORTH ANDROS ISLAND, BAHAMAS

- INTRODUCTION -

For the modeling presented in this thesis, a U. S. Geological Survey code for Heat and Solute Transport in Three Dimensions (HST3D) was used (Kipp, 1987). HST3D is a finite difference, density dependent flow model that simultaneously solves coupled groundwater flow, heat transport, and solute transport equations. This should allow simulation of the mechanisms outlined by Simms (1984) and Whitaker and Smart (1990). HST3D employs the following governing equations:

$$\frac{\partial(n\rho)}{\partial t} = \nabla\bullet\left[\rho\frac{k}{\mu}(\nabla p+\rho g)\right]+q\rho^* \qquad \text{(fluid flow)}$$

$$\frac{\partial}{\partial t}\left[n\rho c_f+(1-n)\rho_s c_s\right]T = \nabla\bullet\left[nK_f+(1-n)K_s\right]I\nabla T+\nabla\bullet nD_H\nabla T-\nabla\bullet n\rho c_f vT+q_H+q\rho^* c_f T^*$$

(heat transport)

$$\frac{\partial(n\rho w)}{\partial t} = \nabla\bullet n\rho D_s\nabla w+\nabla\bullet n\rho D_m I\nabla w-\nabla\bullet n\rho vw+q\rho^* w^* \qquad \text{(solute transport)}$$

where the dependent variables are:

- p is the pressure
- T is the fluid temperature
- w is the solute mass fraction

and the input parameters, source terms and constants are defined as follows:

D_H is the thermal-mechanical dispersion tensor

D_s is the mechanical dispersion tensor

D_m is the effective molecular diffusivity of the solute

I is the identity matrix

K_f is the fluid thermal conductivity

K_s is the solid thermal conductivity

T* is the temperature of the fluid source

c_f is the heat capacity of the fluid

c_s is the heat capacity of the solid phase

g is the gravitational acceleration

k is the permeability tensor

n is the effective porosity

q is the volumetric fluid source rate

q_H is the heat source rate

v is the advective velocity

w* is the solute mass fraction of the fluid source

μ is the fluid viscosity

ρ is the fluid density

ρ_s is the solid phase density

ρ^* is the density of the fluid source

HST3D solves for the dependent variables pressure, temperature, and solute mass fraction through the governing equations linked by velocity, density, and viscosity coupling terms: advective transport depends on interstitial fluid velocity, fluid viscosity depends on temperature and solute mass fraction, and fluid density

depends on temperature, pressure, and solute mass fraction. All simulations presented in this paper were run on a SiliconGraphics Iris Indigo XZ 4000.

- CONCEPTUAL MODEL -

For the purposes of this model, North Andros Island will be considered a strip oceanic island, that is, flow parallel to the long axis of the island is negligible (Anderson, 1976). This allows the model domain to be simplified to a two-dimensional cross section. The simulation region consists of a cross section through the northern Great Bahama Bank and North Andros Island at approximately 25° north latitude. It extends for 155 kilometers in an ENE to WSW direction to 3000 meters water depth (Figure 9). The bank top and platform margins are considered to be specified pressure boundaries, the pressure being the pressure exerted by the overlying water column:

$$P = \rho g h$$

where P is the pressure, ρ is the water density, g is the acceleration of gravity, and h is the height of the water column. It is assumed that the base of the model domain is sufficiently deep that minimal vertical flow occurs and can be modeled as a no-flow boundary.

A grid was chosen so that the element size in the vicinity of North Andros Island was small enough to capture reflux of dense bank brines and possibly the interface between fresh and salt waters. Grid spacing in the horizontal (x) direction was uniform at 5000 meters. The vertical spacing is 5 meters from 0 to 20 meters depth, expanding to a 50 meter spacing from 250 to 3000 meters depth (Figure 10).

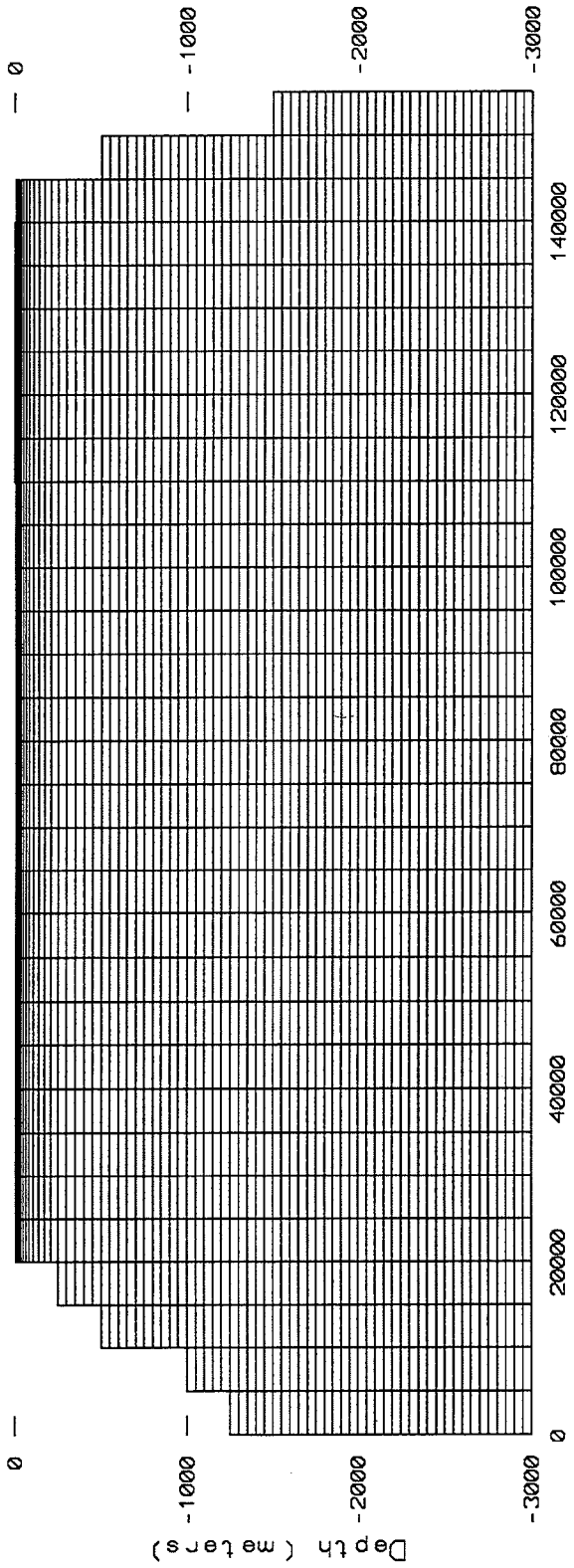

Figure 10. Model grid for HST3D.

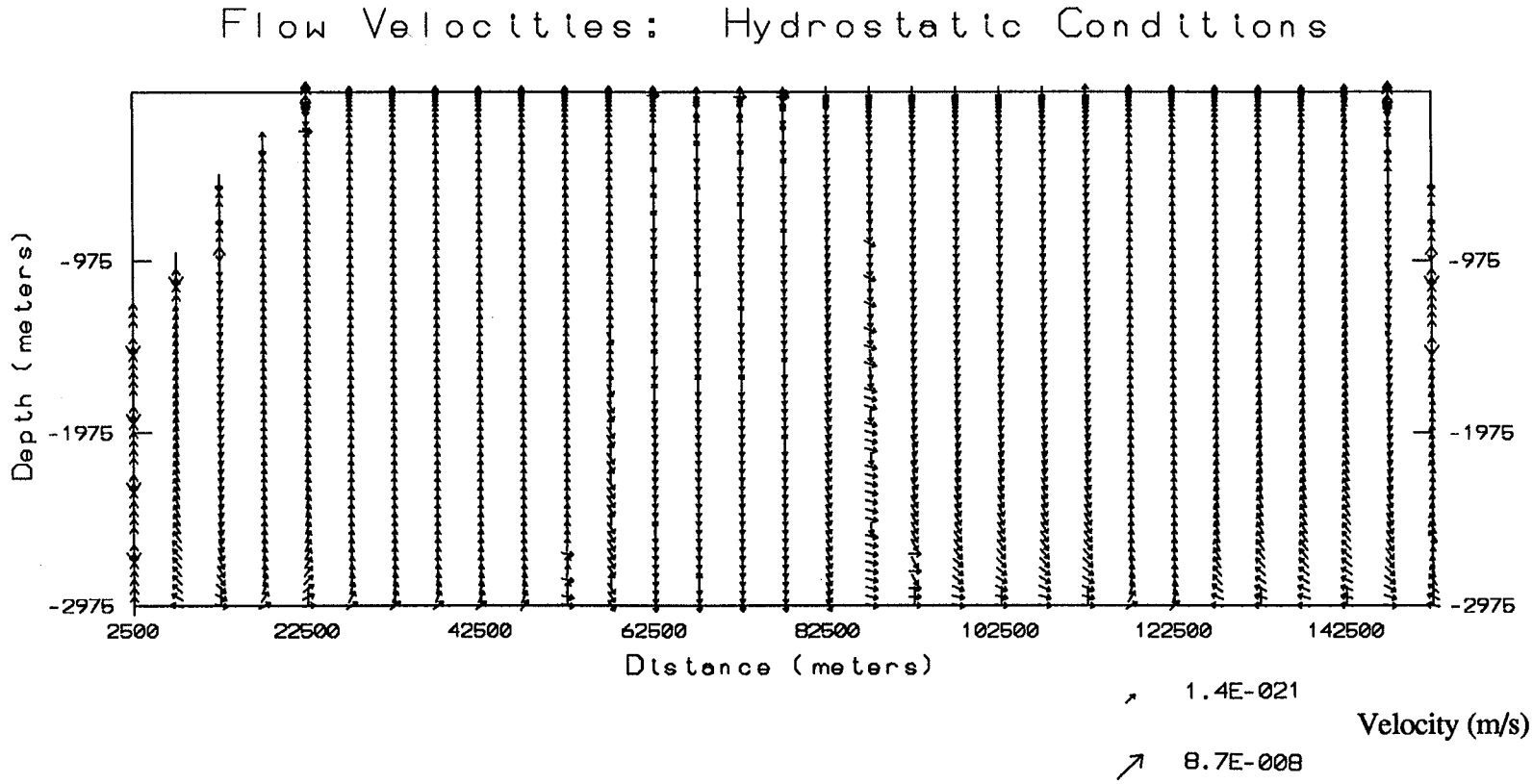

Figure 11. Ground water flow velocities under hydrostatic conditions. Fluid heads are effectively zero everywhere within the model domain under these conditions.

- GROUND WATER FLOW -

Prior to testing mechanisms to drive fluid flow, the model was tested as a simple hydrostatic boundary condition case, where no flow should occur. Initial hydrostatic conditions were calculated and set equal to the boundary conditions. As was expected, hydraulic heads were effectively zero everywhere within the model domain, but small fluid velocities (average of 10^{-12}m/s) were generated. These flow velocities are most likely due to some numerical instability caused by rounding errors (Figure 11). Values chosen for input parameters are shown in Table 1.

Table 1: Parameter Values

Parameter	*Value*	*Reference*
Fluid compressibility	$0.0\ \frac{m^2}{N}$	
Fluid heat capacity†	$4180\ \frac{J}{kg \cdot s}$	CRC Handbook‡
Fluid thermal conductivity†	$0.60\ \frac{J}{m \cdot s \cdot °C}$	CRC Handbook‡
Fluid coefficient of thermal expansion†	$2.5 \times 10^{-4}\ °C^{-1}$	CRC Handbook‡
Porous medium compressibility	$0.0\ \frac{m^2}{N}$	
Porous medium heat capacity†	$2.0 \times 106\ \frac{J}{m^3 \cdot °C}$	CRC Handbook‡
Porous medium thermal conductivity†	$1.7\ \frac{J}{m \cdot s \cdot °C}$	CRC Handbook‡
Geothermal heat flux†	$0.057\ \frac{J}{m^2 \cdot s}$	Kohout, 1967
Longitudinal dispersivity†	5000 m	
Transverse dispersivity†	50 m	

† For heat transport simulations only

‡ *CRC Handbook of Chemistry and Physics* (Weast et al., 1986)

Initial runs were made with purely hydraulic boundary conditions (no heat or solute transport). For these runs, conservative values of 20 and 30 centimeters elevation potential were used for lack of better estimates. A small gradient is invoked across the shallow west bank in order to maintain numerical stability--the pressure had to increase slightly from node to node to prevent vertical velocity oscillations from dominating the flow field. The resulting gradient of 0.001 m/5000 m does not affect the resulting flow field. Within North Andros itself, freshwater recharge percolates through karstic limestone to the water table where it forms a lens up to 35 meters thick (average maximum of 27 meters). Assuming hydrostatic conditions, this translates to a fresh water head approximately 0.5 meters above sea level (Cant and Weech, 1986; and Weech, pers. comm., 1994). Considering that 27 meters is the average maximum thickness of the freshwater lens for Andros Island, and the model domain is in close proximity to the island margin, I have chosen to use a slightly lower value of 0.4 meters of freshwater head.

Results of the initial homogeneous and isotropic run are shown as a velocity plot in Figure 12. High heads within the island dominate the flow field and create a groundwater divide that penetrates the entire thickness of the bank. Increasing the elevation potential across the island between the west bank and TOTO will not generate a net eastward flow under Andros island (as proposed by Whitaker and Smart, 1993) unless the head on the west bank is higher than the fresh water head within the island itself. Since no solute transport is not simulated, no account is taken of the role density differences play in the calculation of freshwater heads.

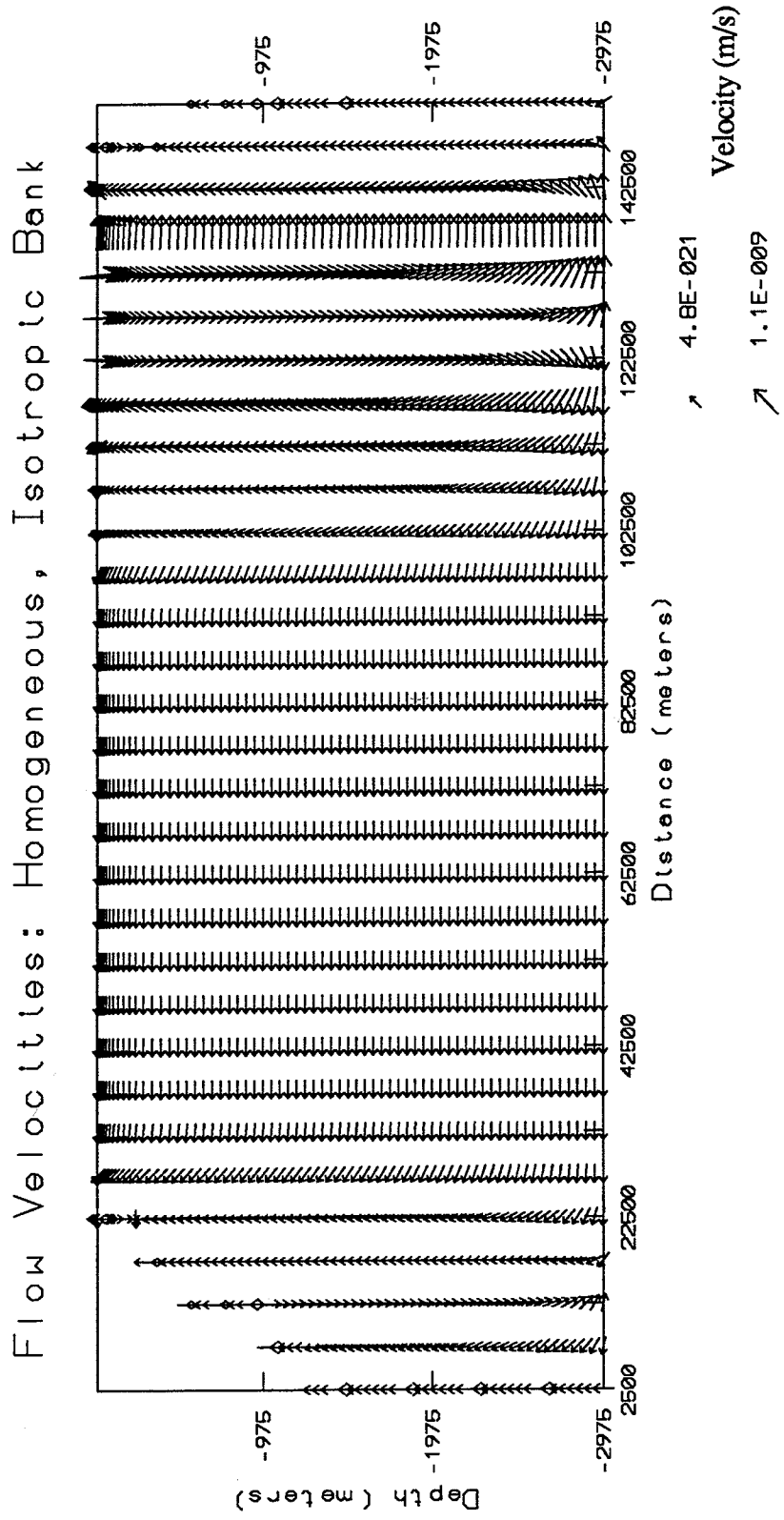

Figure 12. Ground water flow in a homogeneous, isotropic bank with 20 cm elevation potential imposed across North Andros Island.

So far, only a simple case of a completely homogeneous, isotropic carbonate bank has been considered. In the real world, however, such banks do not exist, due not only to the sedimentation process itself, but to subsequent diagenetic alteration. On the basis of the cross section in Figure 9, the model domain can be broken up into porous media zones, each zone having its own set of aquifer and fluid parameters defined explicitly in the model (Figure 13). Hydrogeologic properties were determined for these deposits from core data and discussion of the geology (previous section), and are summarized in Table 2.

Table 2: Hydrogeologic properties for groundwater flow simulations.

Bank heterogeneity	Zone 1			Zone 2			Zone 3		
		Permeability (m^2)			Permeability (m^2)			Permeability (m^2)	
	n	kx	kz	n	kx	kz	n	kx	kz
Homogeneous/ Isotropic	.30	$1x10^{-14}$	$1x10^{-14}$	.30	$1x10^{-14}$	$1x10^{-14}$	.30	$1x10^{-14}$	$1x10^{-14}$
100:1 anisotropy ratio	.35	$1x10^{-11}$	$1x10^{-11}$	.30	$5x10^{-13}$	$5x10^{-15}$	.30	$5x10^{-14}$	$5x10^{-16}$
1000:1 anisotropy ratio	.35	$1x10^{-11}$	$1x10^{-11}$	.30	$5x10^{-12}$	$5x10^{-15}$	.30	$5x10^{-13}$	$5x10^{-16}$

Several heterogeneous runs were made with the goal to reproduce a net eastward flow beneath North Andros Island, as hypothesized by Whitaker and Smart (1993). The first of these used a base elevation potential of 0.2 m across the island (as did the homogeneous/isotropic run), one order of magnitude difference in hydraulic conductivity between porous media zones, and incorporated a 100:1 horizontal to vertical anisotropy ratio. The results of this run are shown in Figure 14a. The largest velocities are concentrated within the island and the uppermost Holocene deposits. Differences in the hydraulic conductivity between the zones

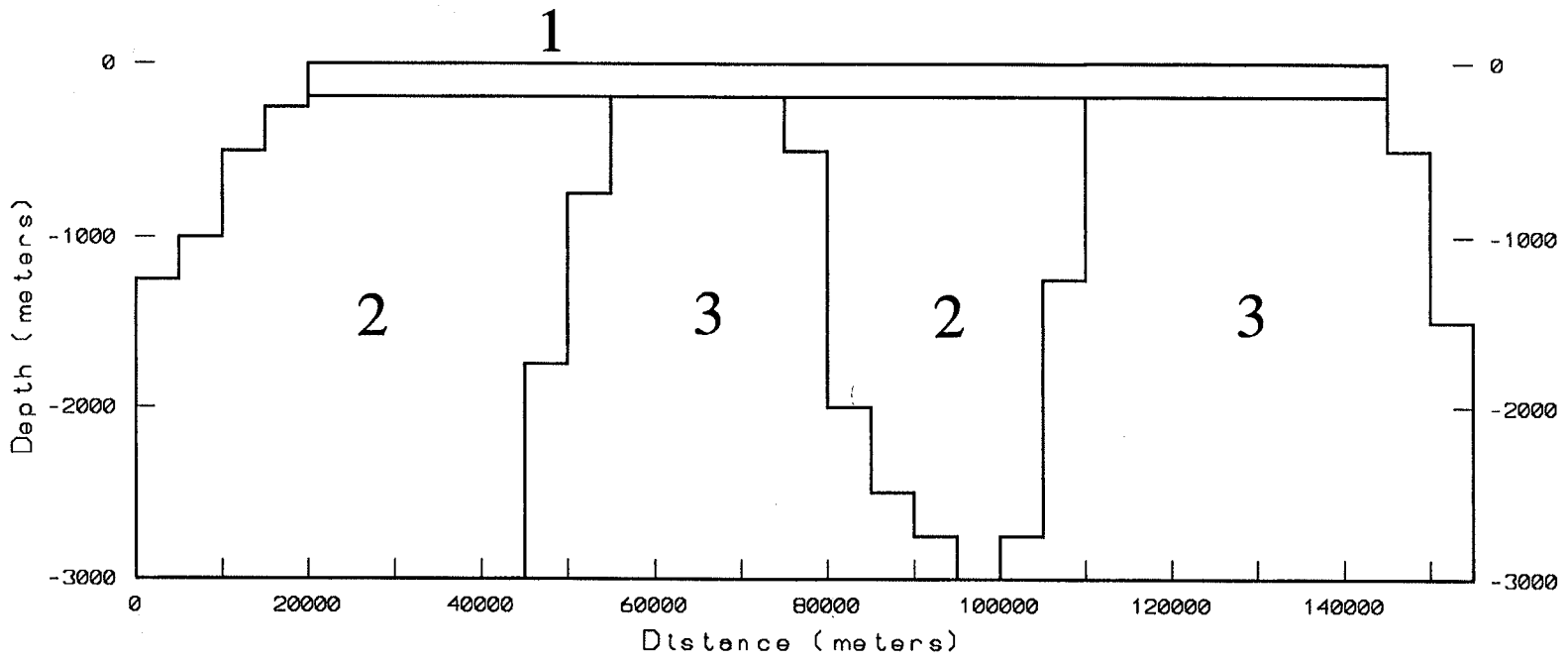

Figure 13. Porous media zones for HST3D. 1) high permeability, high porosity, isotropic Holocene sediments, 2) moderate permeability, anisotropic Straits deposits, 3) relatively low permeability, anisotropic Bank deposits.

are apparent as are small directional changes in velocity at the zone boundaries. The most noticeable change, however, is a result of increasing the anisotropy ratio, which forces greater horizontal flow, and shifts the groundwater flow divide farther to the west. By increasing the anisotropy ratio by one order of magnitude, which may or may not be physically reasonable, through-flow eastward under Andros Island can be generated (Figure 14b). Increasing the elevation potential across the island to 0.3 also generates influx along the western platform margin. The flow regime is then dominated by two areas of high head, creating strong convergent flow at the western bank margin (Figures 14c and d). The groundwater divide in this case is only shifted slightly farther west than with 0.2 m head difference.

Changing the magnitude of hydraulic conductivity (leaving the relative differences constant, Figures 15 and 16), and of changing the relative hydraulic conductivities (Figure 17) had predictable results. Increasing the hydraulic conductivity by one order of magnitude uniformly in the model domain raised the flow velocities by one order of magnitude. Likewise, lowering the hydraulic conductivity uniformly lowered flow velocities (Table 3).

Changing the relative hydraulic conductivity between zones deflects the velocities at the zone boundaries--as the difference in hydraulic conductivity becomes larger, flow is diverted out of the lower conductivity units.

Taking realistic salinity and temperature distribuitons into account,the island head actually can be lower than that of the western bank margin. The end result of these conditions is a net eastward groundwater flow beneath Andros Island even in the absence of bank heterogeneity. The results of these runs are not shown because the boundary conditions used for groundwater flow were calculated for a heat transport model, and the resulting flow field is not resonable. The pressure distribution generated was used as initial conditions for heat transport simulations.

Table 3: Flow Velocities

	Velocity $\left(\frac{m}{s}\right)$		
	minimum	maximum	average
20 cm elevation potential:			
homogeneous/isotropic	4.8×10^{-23}	1.1×10^{-11}	1.5×10^{-12}
100:1 anisotropy ratio	4.1×10^{-20}	8.5×10^{-9}	2.4×10^{-10}
1000:1 anisotropy ratio	4.1×10^{-20}	8.5×10^{-9}	2.6×10^{-10}
30 cm elevation potential:			
100:1 anisotropy ratio	4.1×10^{-20}	1.3×10^{-8}	4.1×10^{-10}
1000:1 anisotropy ratio	4.1×10^{-20}	1.3×10^{-8}	4.5×10^{-10}
Low conductivity:			
100:1 anisotropy ratio	4.1×10^{-21}	8.5×10^{-10}	2.4×10^{-11}
1000:1 anisotropy ratio	4.1×10^{-21}	8.5×10^{-10}	2.6×10^{-11}
High conductivity :			
100:1 anisotropy ratio	4.1×10^{-19}	8.5×10^{-8}	2.4×10^{-9}
1000:1 anisotropy ratio	4.1×10^{-19}	8.5×10^{-8}	2.6×10^{-9}
3 orders magnitude relative K:			
100:1 anisotropy ratio	4.1×10^{-20}	8.5×10^{-9}	2.4×10^{-10}
1000:1 anisotropy ratio	4.1×10^{-20}	8.5×10^{-9}	2.4×10^{-10}

Figure 14. Ground water flow velocities in a heterogeneous, anisotropic carbonate platform, a) using 20 cm elevation potential across Andros Island and a 100:1 horizontal to vertical anisotropy ratio, b) using 20 cm elevation potential across Andros Island and a 1000:1 horizontal to vertical anisotropy ratio, c) using a 30 cm elevation potential across Andros Island and a 100:1 horizontal to vertical anisotropy ratio, and d) using a 30 cm elevation potential across Andros Island and a 1000:1 horizontal to vertical anisotropy ratio.

Figure 15. Ground water flow velocities in a low conductivity bank resulting from a) a 20 cm elevation potential across Andros Island and a 100:1 horizontal to vertical anisotropy ratio, and b) a 20 cm elevation potential across Andros Island and a 1000:1 horizontal to vertical anisotropy ratio.

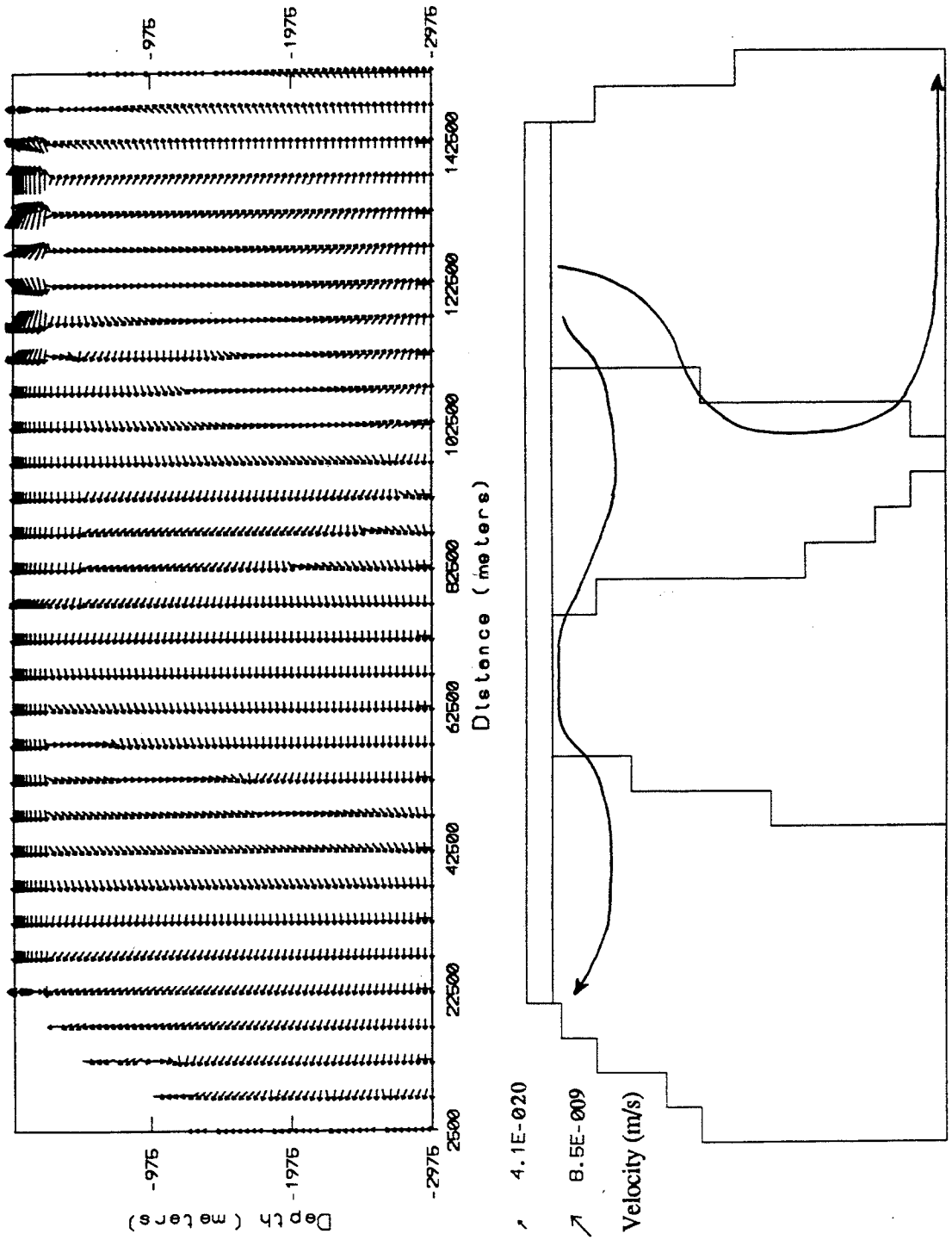
-975
-1975
-2975
25000
42500
62500
82500
102500
122500
142500
Distance (meters)
Depth (meters)
4.1E-020
8.5E-009
Velocity (m/s)

Figure 14a.

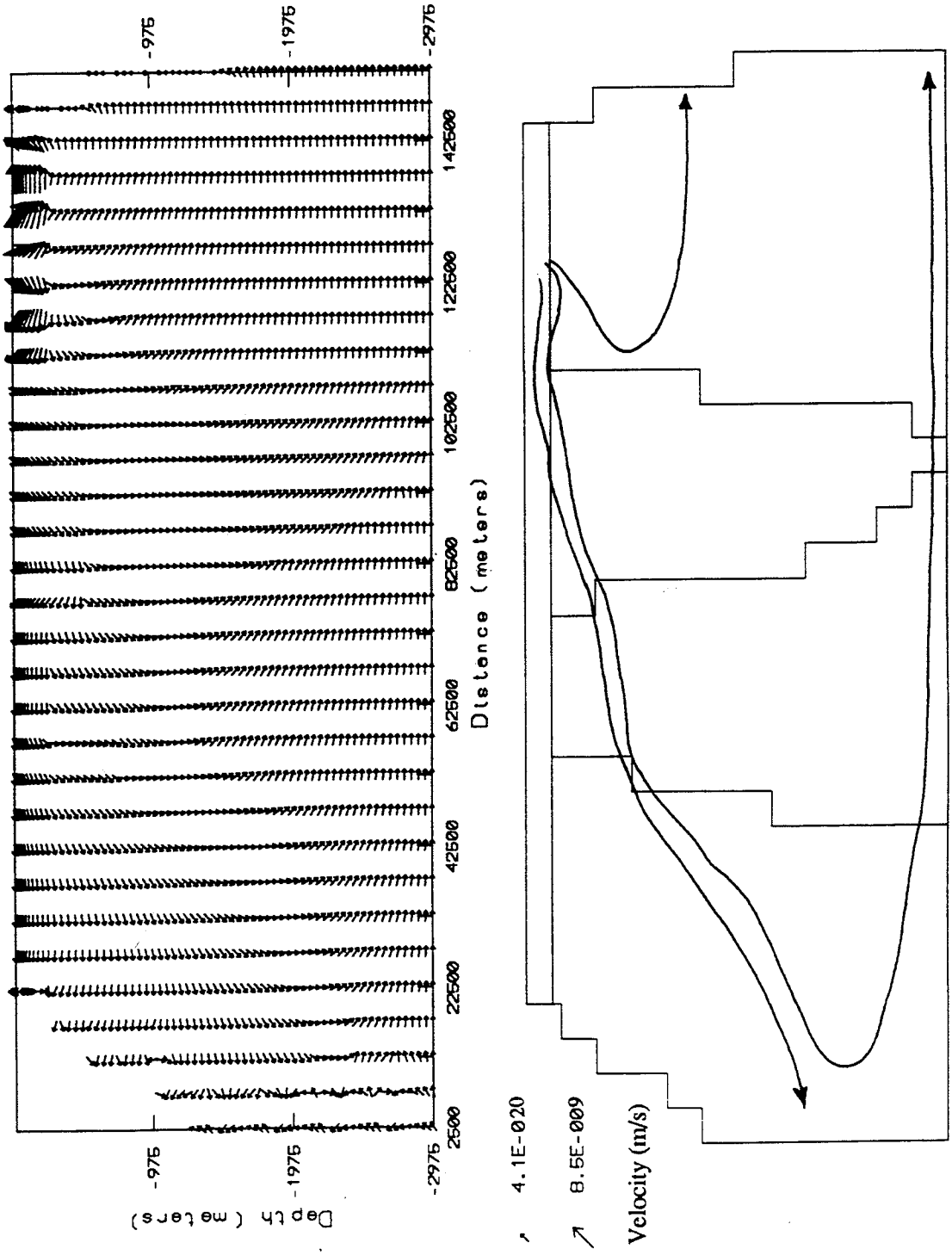
-975
-1975
-2975
Depth (meters)
-975
-1975
-2975
2500
22500
42500
62500
82500
102500
122500
142500
Distance (meters)
4.1E-020
8.5E-009
Velocity (m/s)

Figure 14b.

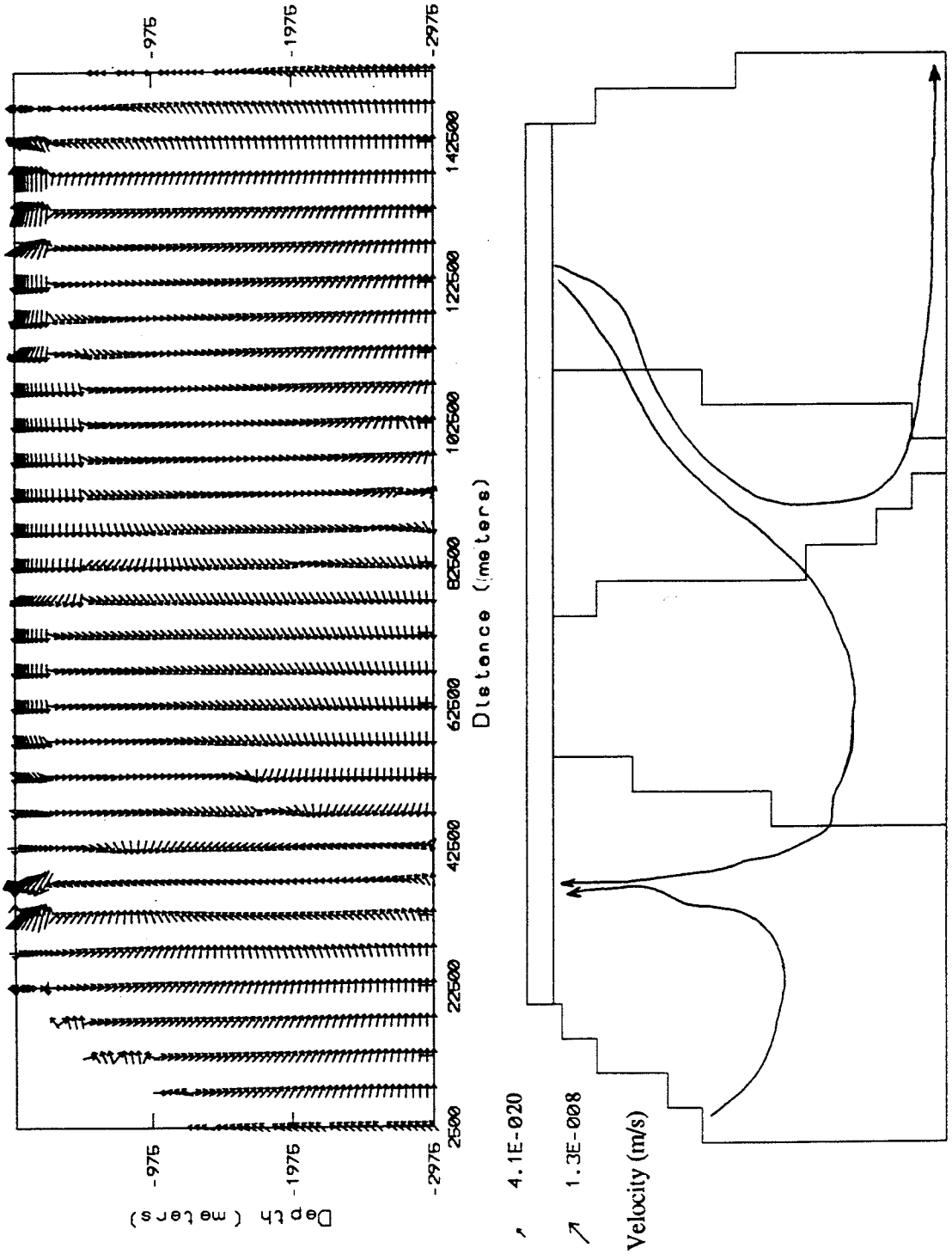
-975
-1975
-2975
Depth (meters)
2500
42500
82500
122500
142500
Distance (meters)
4.1E-020
1.3E-008
Velocity (m/s)

Figure 14c.

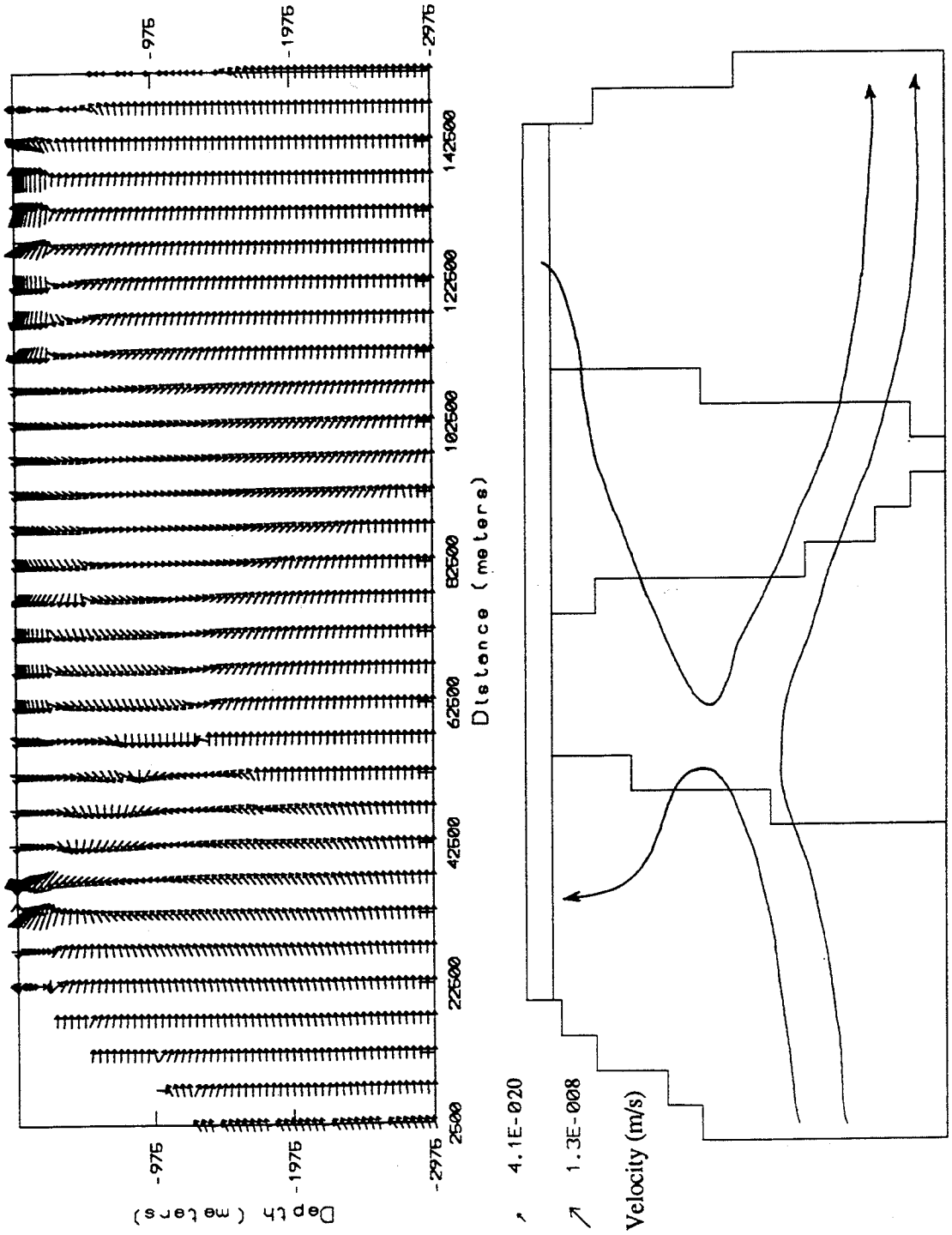
-975
-1975
-2975
Depth (meters)
2500
22500
42500
62500
82500
102500
122500
142500
Distance (meters)
4.1E-020
1.3E-008
Velocity (m/s)

Figure 14d.

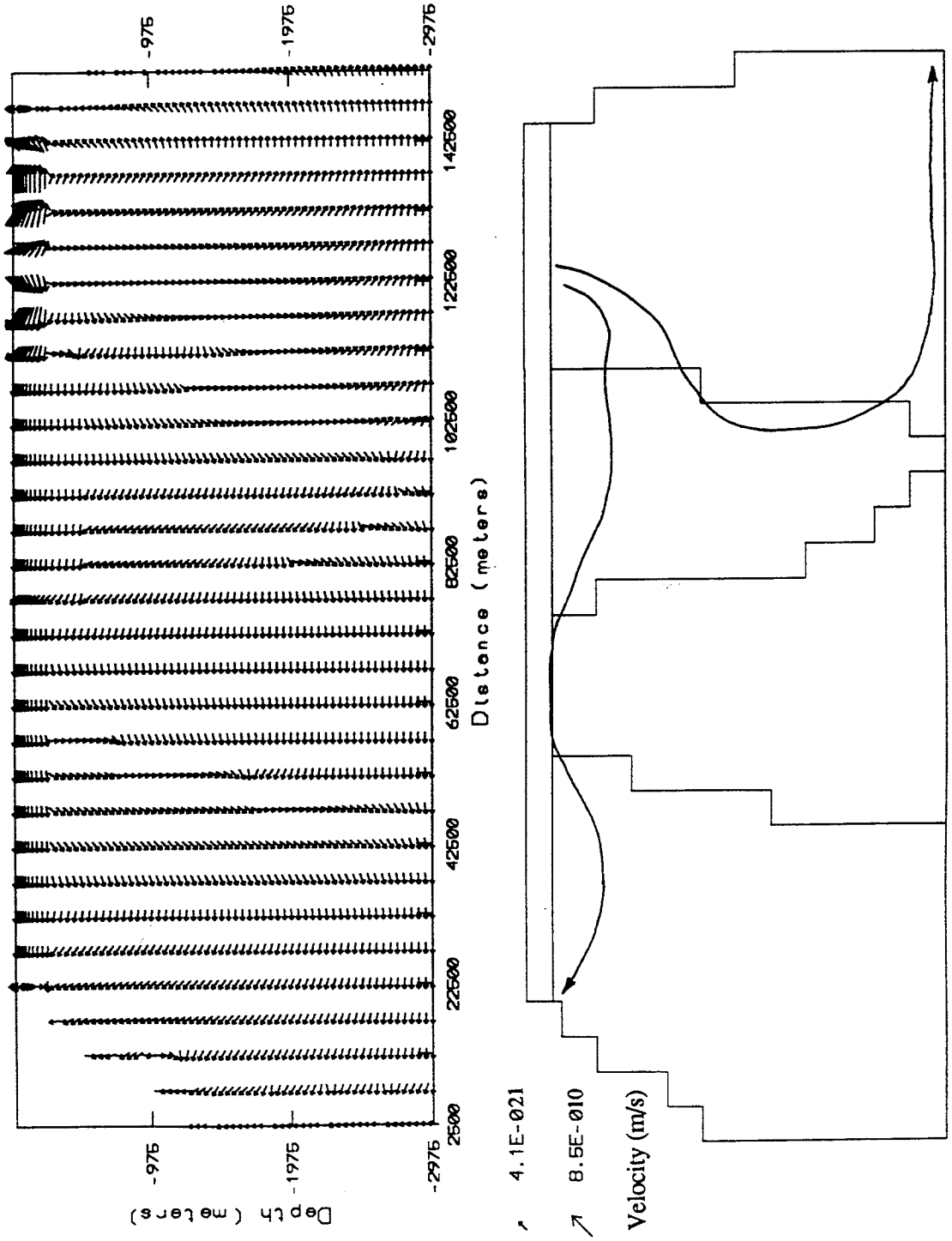
-975
-1975
-2975
Depth (meters)
2500
22500
42500
62500
82500
102500
122500
142500
Distance (meters)
4.1E-021
8.5E-010
Velocity (m/s)

Figure 15a.

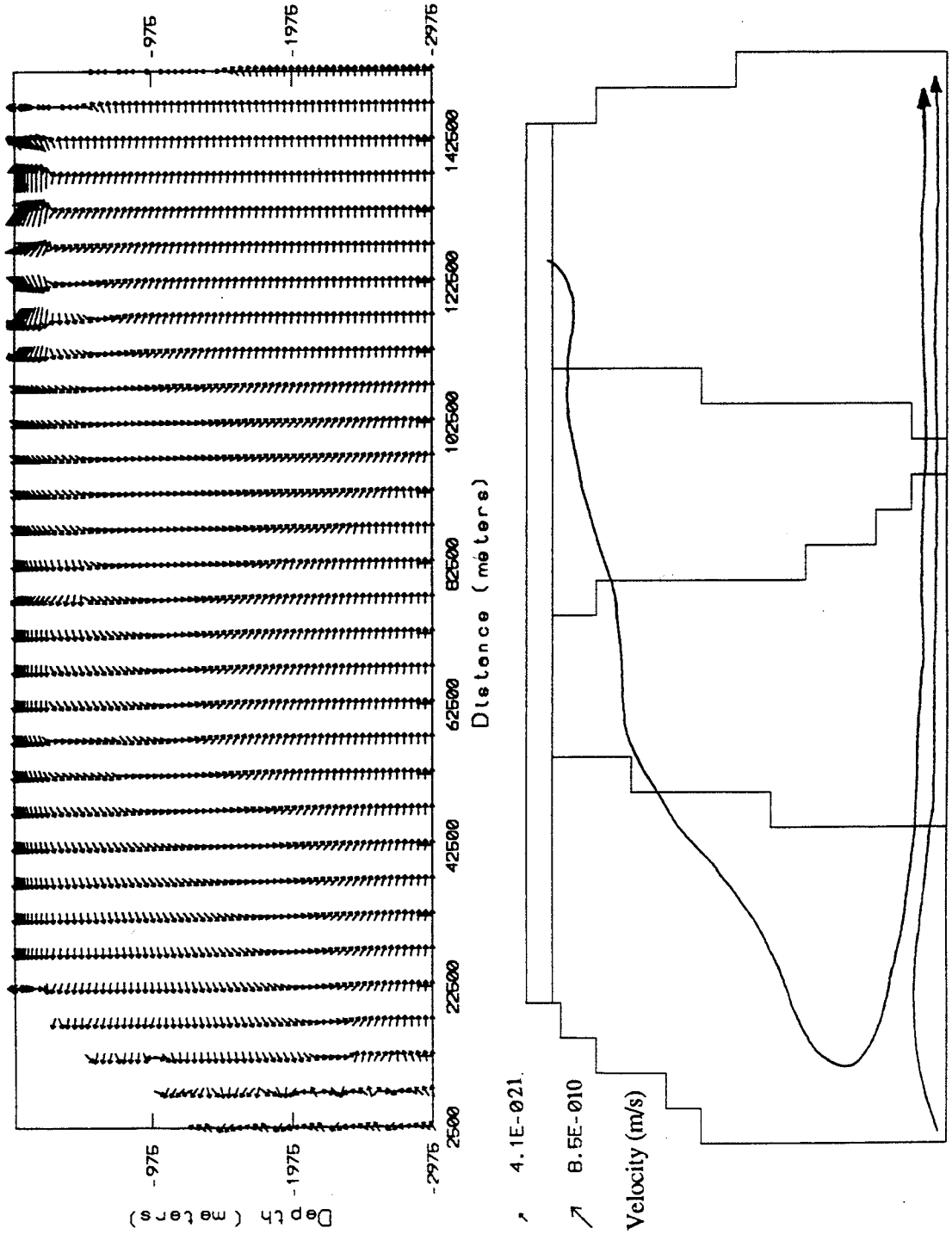
-975
-1975
-2975
2500
22500
42500
62500
82500
102500
122500
142500
Distance (meters)
Depth (meters)
4.1E-021
8.5E-010
Velocity (m/s)

Figure 15b.

Figure 16. Ground water flow velocities in a high conductivity bank resulting from a) a 20 cm elevation potential across Andros Island and a 100:1 horizontal to vertical anisotropy ratio, and b) a 20 cm elevation potential across Andros Island and a 1000:1 horizontal to vertical anisotropy ratio.

Figure 17. Flow velocities in the bank with 3 orders of magnitude difference in hydraulic conductivity between zones and a) 20 cm elevation potential across Andros Island and a 100:1
anisotropy ratio, and b) 20 cm elevation potential, and a 1000:1 anisotropy ratio.

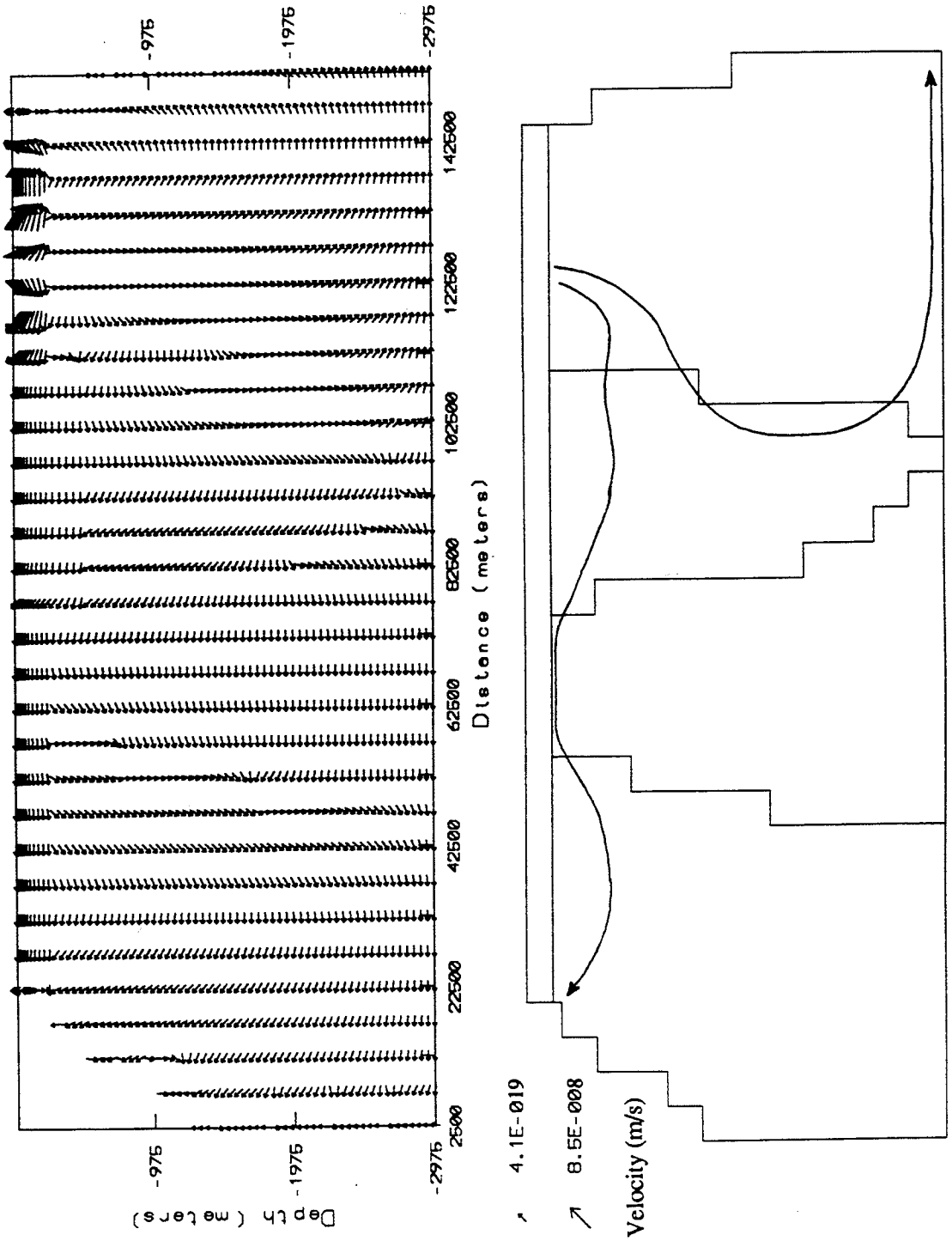
-975
-1975
-2975
Depth (meters)
2500
22500
42500
62500
82500
102500
122500
142500
Distance (meters)
4.1E-019
8.5E-008
Velocity (m/s)

Figure 16a.

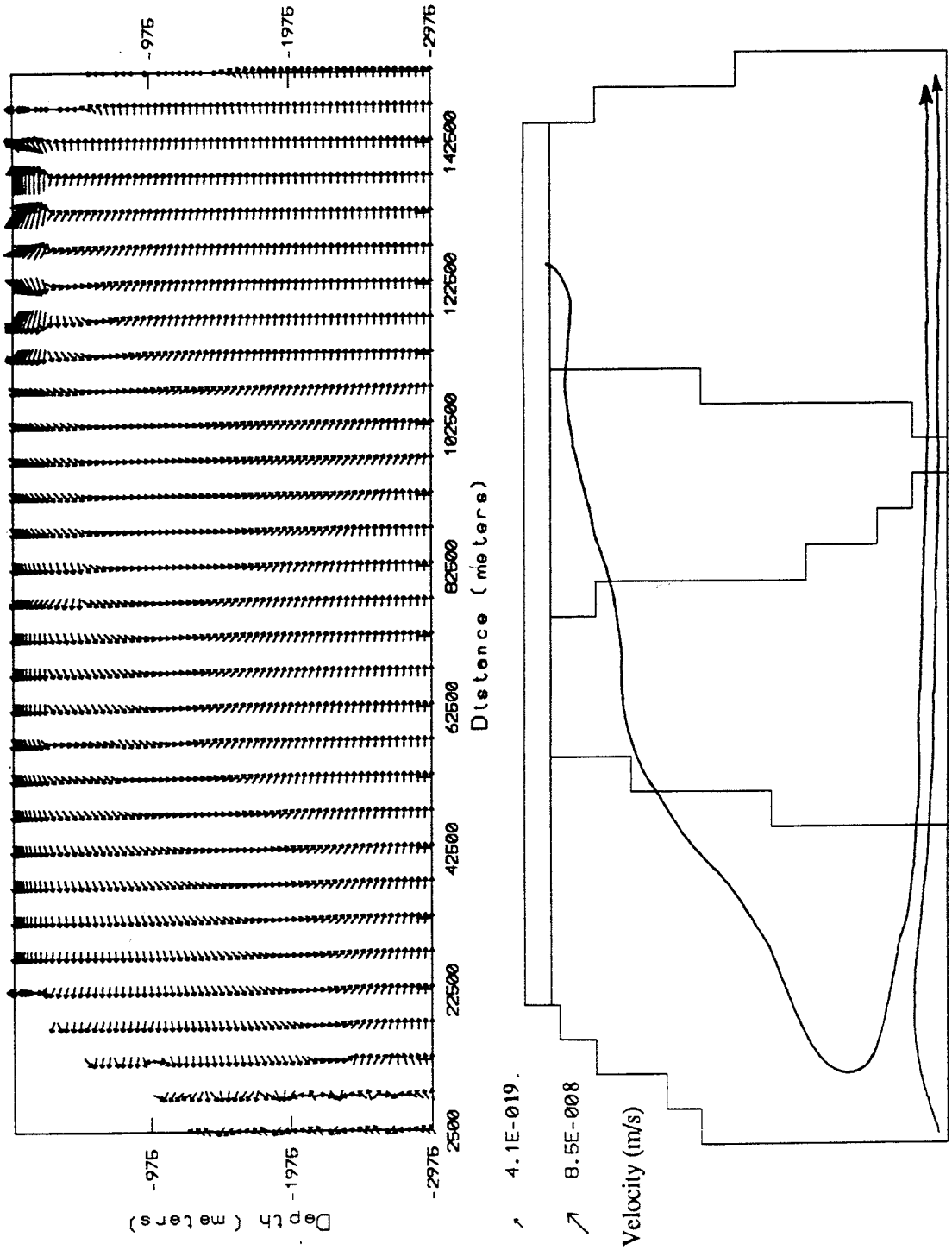
-975
-1975
-2975
2500
22500
42500
62500
82500
102500
122500
142500
Distance (meters)
Depth (meters)
4.1E-019
8.5E-008
Velocity (m/s)

Figure 16b.

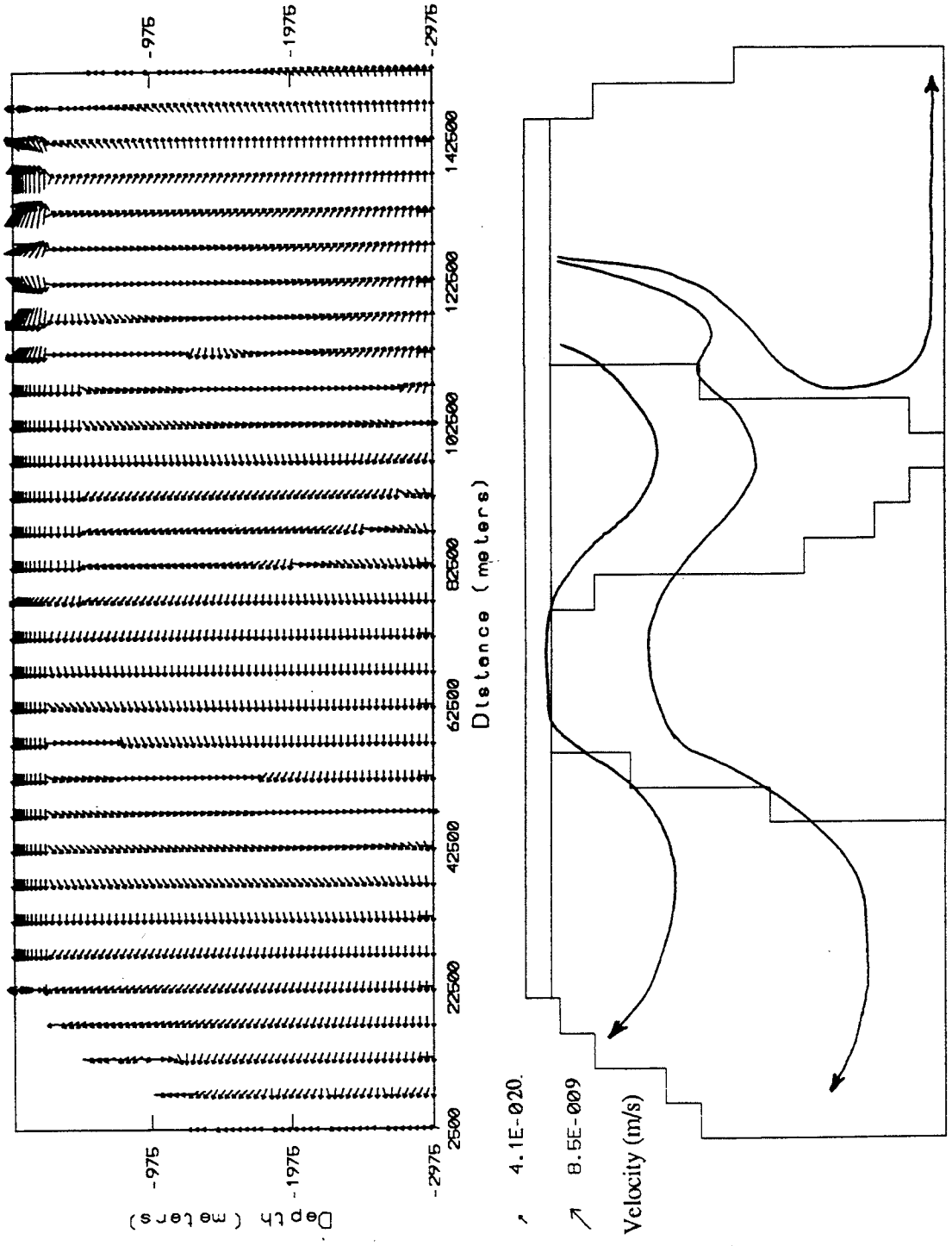
-975
-1975
-2975
2500
42500
82500
122500
142500
Distance (meters)
Depth (meters)
4.1E-020.
8.5E-009
Velocity (m/s)

Figure 17a.

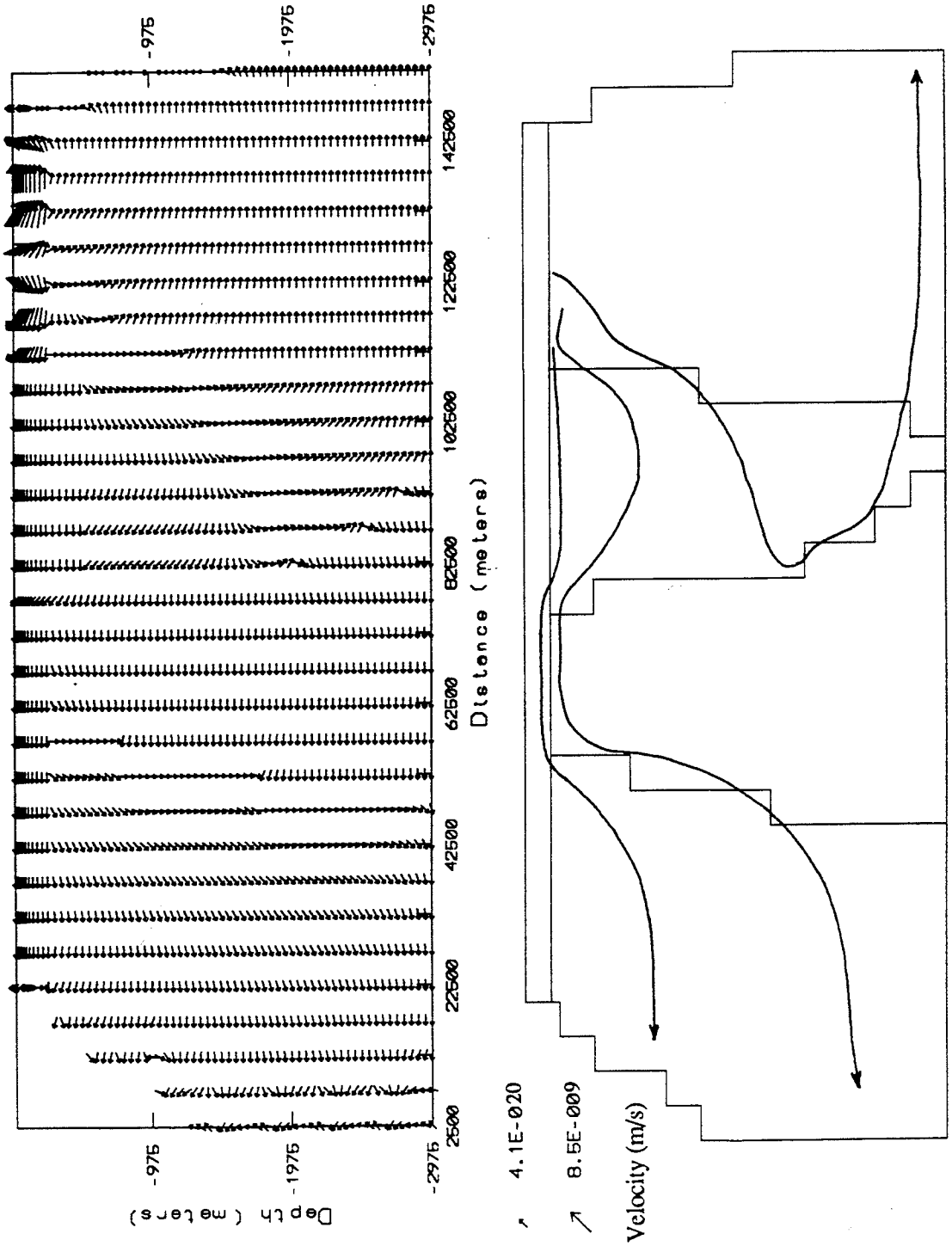
-975
-1976
-2976
Depth (meters)
2500
42500
82500
122500
142500
Distance (meters)
4.1E-020
8.5E-009
Velocity (m/s)

Figure 17b.

- HEAT TRANSPORT -

Heat transport simulations were run in a transient mode, allowing the model to adjust the time step automatically to shorten computing time. Before heat transport could be simulated, a suitable initial pressure distribution had to be generated. In order to do this, a groundwater flow system was set up with the same boundary conditions as the groundwater flow simulations in the previous section, but with the pressure adjusted for variable water density (density as a function of temperature; Knauss, 1978). The resulting flow system is not realistic and generates strong upward velocities at the bank margins, where the densities used in the boundary pressure calculation were significantly higher at depth than the constant density assumed in the groundwater flow model. In theory, however, the resulting pressure distribution will be close to a reasonable initial pressure distribution for the heat transport simulation. For a first attempt, an initial temperature gradient was specified within the bank corresponding to an open ocean temperature gradient, and a heat flux of .057 $\frac{J}{m^2 \cdot s}$, consistent with a 30°/1000 m geothermal gradient and 1.7 $\frac{J}{m \cdot s \cdot °C}$ thermal conductivity was invoked along the base of the model domain (see Table 2 for heat transport input parameters).

This simulation ran into problems quickly, as the heat flux was unable to cope with cold water inflow at the base of the model. High temperature oscillations began to form on the lower portion of the eastern platform margin, eventually resulting in nodes of ice immediately adjacent to 100°C + temperatures, at which point the model crashed. All of this occurred within about 500 years of simulation time.

In HST3D, associated inflow temperatures are given where pressures are specified along the bank margin. The assumption in the previous simulation was

that water within the bank was colder with depth. In reality, the lower portions of the bank margins are not exposed to open ocean waters. The model domain had to be cut off to keep the modeling domain size within the realm of practicality, and the waters on these margins are warmed by the geothermal heat flux. If it can be assumed that these parts of the bank margins (below 1250 meters water depth in the west and below 1500 meters water depth in the east) are deep enough to be considered no-flow boundaries, the problem of determining the temperatures at these locations prior to the simulation becomes moot. Closer examination of the groundwater flow output from the previous section shows that in these simulations, flow velocities oscillated in a vertical direction at these locations, producing a net flow velocity of zero consistent with a no-flow boundary. The model was re-run with a new initial pressure distribution and no-flow boundaries. The same problems occurred as before, but it took longer simulation times to reach them.

This last run was also tried with a specified temperature along the lower parts of the bank margins (along the no-flow portions of the bank). The temperatures used assumed a ocean water temperature consistent with an ocean thermal gradient at the uppermost layer, increasing within the bank at a rate of 1.5°C/50 meters. Again, the simulation ran slightly longer, but was no real improvement over the previous attempts.

The next series of simulations involved playing with the initial temperature distribution. The previous two attempts involved a fixed temperature gradient based on gradients in open ocean water, but within the carbonate platform, water should become warmer with depth in response to a geothermal heat flux. The simulations described above were modified to use an initial temperature distribution generated by analogy with a simple boundary value groundwater flow simulation. The boundary conditions for the subsequent coupled model were set to

fixed temperatures expected along the base and margins of the platform. These results were somewhat better--the model still only ran to 50 to 500 years of simulation time and created high temperature fluctuations on the bank margins, but there were some vague convection cells resembling Kohout convection beginning to develop as well.

A better solution still was obtained by increasing dispersivity values. The initial dispersivity values of α_L = 50 m and α_t = 0 m were chosen to try to preserve sharp temperature and solute fronts (Voss and Souza, 1987), but these values are much too small to satisfy the stability criterion given by the grid Peclet number. New values of 5000 m and 50 m were chosen for α_L and α_t respectively. A plot of the temperature output for the last of these simulations is shown in Figure 18.

The last modeling attempt involved modifying the horizontal grid spacing to try to spread out the temperature gradient over more elements. Changing the nodal spacing from 5000 meters to 2500 meters increased the size of the problem considerably and had the effect of doubling the computing time necessary for the simulation. Simulation times reached the order of 500 years in just over two days (real time) before the model crashed. In this run, however, the cause of the crash was not huge temperature variations, but failure to converge to a solution within the required number of iterations.

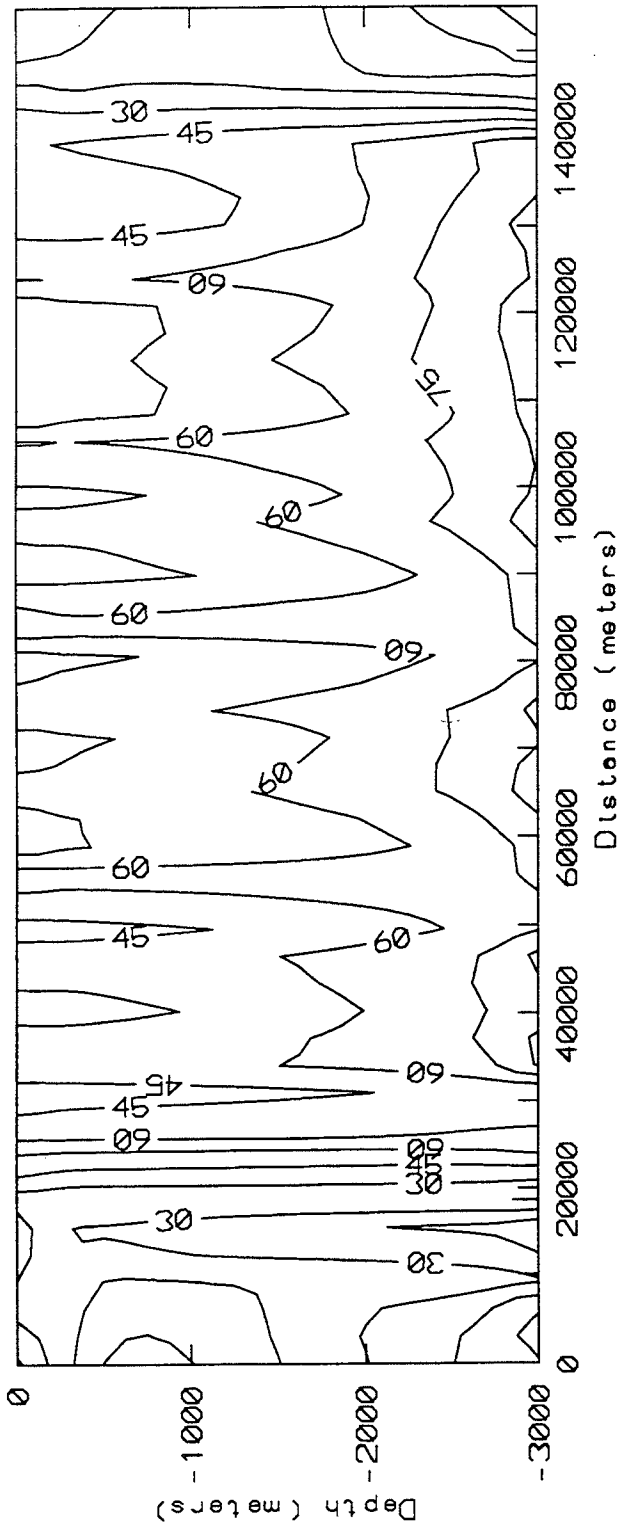

Figure 18. Temperature distribution at approximately 200 years.

Chapter 5

IMPLICATIONS FOR DOLOMITIZATION

The mass flux of solute through a flow system is the key to diagenesis within that system. The magnesium mass flux is defined as:

$$q \times C$$

where q is defined as the Darcy velocity, $\left[\frac{\text{vol.}}{m^2 \cdot t}\right]$ and C is the molar concentration of solute, $\left[\frac{\text{moles}}{L}\right]$. If we consider ordinary seawater as a potentially dolomitizing solution, the magnesium mass flux may be calculated by the following (assuming a porosity of 0.3 and a sample velocity of $8.5 \times 10^{-9} \frac{m^3}{m^2 \cdot s}$):

$[Mg^{++}]$ in seawater = 1.29 g/L = .053 mol/L (Stumm and Morgan, 1981)

$$q = \left[8.5 \times 10^{-9} \frac{m^3}{m^2 \cdot s}\right] \times (0.3) \times \left[\frac{1000\ L}{m^3}\right] = 2.55 \times 10^{-6} \frac{L}{m^2 \cdot s}$$

$$= 80.4 \frac{L}{m^2 \cdot yr}$$

$$Mg^{++} \text{ mass flux} = \left[80.4 \frac{L}{m^2 \cdot yr}\right] \times \left[\frac{.053\ mol}{L}\right] = 4.3 \frac{mol}{m^2 \cdot yr}$$

The amount of time required to completely dolomitize a 1 km x 1 km x 1 km block of limestone (all calcite), with 30% porosity can be calculated from the mass fluxes:

$$1\ km^3\ CaCO_3 = 1 \times 10^9\ m^3\ CaCO_3$$

$$\times 0.6 = 6.0 \times 10^8\ m^3\ CaCO_3 \text{ (accounting for porosity)}$$

(assuming a specific gravity = 2.71 g/cm^3; Mottana et al.,1978)

$$2.71\ \frac{g}{cm^3} \times \frac{1 \times 10^6\ cm^3}{m^3} \times (6.0 \times 10^8\ m^3\ CaCO_3) \times \frac{1\ mole\ CaCO_3}{100.09\ g\ CaCO_3}$$

$$= 1.62 \times 10^{13}\ moles\ CaCO_3$$

Thus, 1.62×10^{13} moles of magnesium are needed:

$$4.3\ \frac{moles\ Mg^{++}}{m^2 \cdot yr} \times (1 \times 10^6\ m^2) \times (1.62 \times 10^{13}\ moles\ Mg^{++})$$

$$= 4 \times 10^6\ years$$

Table 4 summarizes the Darcy velocities and magnesium mass fluxes calculated for the heterogeneous simulations in this study (excluding high and low conductivity extremes), and the results of Simms (1984) and Kaufman (1994). Kaufman used slightly higher porosities than assumed in this study (0.4 to 0.55), and permeabilities that vary as a function of porosity. Kaufman's model assumed a range of permeability for platform limestones of 0.3 to 30 millidarcies (3×10^{-16} to $3 \times 10^{-14}\ m^2$) and 100 to 3×10^5 millidarcies (1×10^{-10} to $3 \times 10^{-7}\ m^2$) for reefal limestones. Both the velocities and mass fluxes computed in this study are comparable in magnitude to Simms and Kaufman's results and similarly are sufficient to dolomitize the platform over long periods of time. Like Simms and Kaufman, this study found the highest velocities (and therefore the highest mass

fluxes) to be directly beneath the island. These velocities would probably be enhanced in a simulation which accounted for solute transport and buoyant circulation associated with an actual mixing zone, which has been thought to be a location where massive dolomitization can occur. The area directly beneath Andros Island is described as a "mixing zone", even though no solute transport was modeled.

Table 4: Representative Darcy velocities and mass fluxes

Process	Darcy Velocity, $\left[\frac{m}{yr}\right]$	Mg Mass Flux, $\left[\frac{moles}{m^2 \cdot yr}\right]$
Coastal Flows		
Mixing Zone (high vel.)	80-123	4-7
Seawater Circulation (avg. vel.)	2-3	0.1-0.2
Simms (1984)	5-20 (Mixing Zone) 0.5-3 (Seawater Circ.)	
Kaufman (1994)		0.4-5†

† Indicates a range of results for the flow systems considered in this research. High end corresponds to reflux, low end is for Kohout convection.

Chapter 6

CONCLUSIONS

Sensitivity analysis on stable groundwater flow systems driven by elevation potential alone yield the expected outcome. Anisotropy within the bank drives flow more horizontally while bank heterogeneity causes velocity deflection around lower permeability units and channelizes flow into high permeability units. Lowering or raising the overall hydraulic conductivity of the system lowers or raises the groundwater flow velocities by the same order of magnitude. Increasing the relative differences in hydraulic conductivity between the porous media zones results in increasing the channelization of fluids in higher permeability zones.

Magnesium mass fluxes within the Bahama Bank are capable of massive dolomitization, although require long time periods (>10^6 years; Kaufman, 1994). The rates and extent of dolomitization within the platform depend on the locations of high mass fluxes of magnesium. Here, after evaluating only flow due to elevation potential, the highest velocities and mass fluxes were found in the mixing zone.

Based on these modeling results, some predictions can be made about the location of digenetic features (or the lack thereof). Zones of high flow velocity, like zones of convergent flow, or flow driven by steep gradients as are found in the vicinity of the island/mixing zone, are also zones of high mass fluxes. In general, high mass fluxes will lead to enhanced cementation if an adequate amount of $CaCO_3$ is supplied. If the high flow velocities are associated with (or result from) either mixed waters or rapid salinity changes, the saturation state of the water with respect to the carbonate minerals could change, resulting in extensive dissolution

(Badiozamani, 1973). Solution caverns thought to be the result of mixing zone dissolution are common in carbonate platforms, as in the Yucatan Peninsula (Stoessell et al., 1989). The highest velocities found in these modeling results are in the vicinity of Andros Island, where flow is driven by a steep gradient, and in the porous, high permeability Holocene deposits on the uppermost part of the platform. Although no solute transport was simulated here, the zone of high velocity flow directly beneath Andros Island is also a mixing zone, thus cavernous porosity could be expected in these zones. The high permeability Holocene sediments have high original porosity and are probably undergoing early cementation. Strong convergent flow was only produced in simulations with a high elevation potential invoked across the island so that two local highs dominate the flow field (Figures 13c and 13d). Convergent flow on the bank margin in this scenario could lead to enhanced cementation.

Low flow velocities are not capable of delivering large enough quantities of carbonate material to extensively cement the rock, unless operational over long periods of time. Areas of the bank with low flow velocities may be areas where primary mineralogy, porosity, and fabrics are preserved. The lowest flow velocities in the model domain are in the low permeability zones and areas where the flow is diverging. Divergent flow is most common to the groundwater divides, and the location of these divides is highly dependant on bank heterogeneity and anisotropy.

The modeling project so far has only considered a constant sea level and modern platform geometry. A rise in sea level submerging the entire platform would destroy the freshwater lens and the restricted shelf environment (where evaporative brines form), and would lessen or completely remove the elevation

potential across the bank. Heat flow within the platform would be the only remaining force to drive fluid flow.

A sea level fall resulting in complete emergence of the shelf may raise the elevation potential across the bank, both by enhancing the Gulf Stream, and by creating a larger obstruction to ocean circulation. The fresh water lens would be at least temporarily destroyed, and no evaporative brines could form...Even without the shallow shelf for water to pile up on, cross platform flow due to elevation potential could be increased.

All attempts at heat transport simulation to date have failed to produce meaningful results, even after reducing the grid spacing and time step size. The discretization of the system as it stands will probably be insufficient to capture sharp temperature gradients or a freshwater/saltwater interface, not to mention a transition zone. SUTRA requires at least 5 elements over which to spread a transition zone (Voss and Souza, 1987) and from every indication, HST3D will require even smaller nodal spacing, shorter time steps, and more time (Ghassemi et al., 1990 and 1993).

Before a final analysis of the flow system with respect to dolomitization can be made, heat and solute transport must be accounted for, as both of these processes are capable of driving large quantities fluid through carbonate platforms.

REFERENCES

Adams, J. E., and Rhodes, M. L., 1960, Dolomitization by seepage refluxion. American Association of Petroleum Geologists Bulletin, v. 44, no. 12, p. 1912-1920.

Aharon, P., Socki, R. A., and Chan, L., 1987, Dolomitization of atolls by sea water convection flow: test of a hypothesis at Niue, South Pacific. Journal of Geology, v. 95, p. 187-203.

Anderson, M. P., 1976, Unsteady groundwater flow beneath strip oceanic islands. Water Resources Research, v. 12, no. 4, p. 640-644.

Badiozamani, K., 1973, The dorag dolomitization model--application to the Middle Ordovician of Wisconsin. Journal of Sedimentary Petrology, v. 43, no. 4, p. 965-984.

Baker, P. A. and Kastner, M., 1981, Constraints on the formation of sedimentary dolomite. Science, v. 213, p. 214-216.

Bathurst, R. G. C., 1975, Carbonate Sediments and their Diagenesis. Elsevier Scientific Publishing Co., Amsterdam. 658 p.

Boggs, S., 1987, Principles of Sedimentology and Stratigraphy. Merrill Publishing Co., Columbus, OH, p. 82-87.

Butler, G. P., 1969, Modern evaporite deposition and geochemistry of coexisting brines, the sabkha, Trucial Coast, Arabian Gulf. Journal of Sedimentary Petrology, v. 39, p. 70-89.

Cant, R. V., and Weech, P. S., 1986, A review of the factors affecting the development of Ghyben-Hertzberg lenses in the Bahamas. Journal of Hydrology, v. 84, p. 333-343.

Carpenter, A. B., 1980, The chemistry of dolomite formation I: the stability of dolomite. *In* Zenger, D. H., Dunham, J. B., and Ethington, R. L. (eds.), Concepts and Models of Dolomitization. Society of Economic Paleontologists and Mineralogists Spec. Pub. #28, p.111-121.

Deffeyes, K. S., Lucia, F. J., and Weyl, P. K., 1965, Dolomitization of recent and Plio-Pleistocene sediments by marine evaporite waters on Bonaire, Netherlands Antilles. *In* Pray, L. C. and Murray, R. C. (eds.), Dolomitization and Limestone Diagenesis. Society of Economic Paleontologists and Mineralogists Spec. Pub. #13, p. 71-88.

Eberli, G. P., and Ginsburg, R. N., 1987, Segmentation and coalescence of platforms, Tertiary, NW Great Bahama Bank. Geology, vol 15, p. 75-79.

Eberli, G. P., and Ginsburg, R. N., 1989, Cenozoic Progradation of NW Great Bahama Bank--A record of lateral platform growth and sea-level fluctuations. *In* Crevello, P. D. et al., (eds.) Controls on Carbonate Platform and Basin Evolution. Society of Economic Paleontologists and Mineralogists Spec. Pub. #44, p. 339-355.

Eberli, G. P., McNeill, D. F., and Swart, P. K., 1992, The Bahamas transect: Neogene/Quaternary sea-level fluctuations and fluid flow in a carbonate platform. Ocean Drilling Project Proposal #412, addendum 2.

Freeze, R. A., and Cherry, J. A., 1979, Groundwater. Prentice Hall, Englewood Cliffs, NJ, 604p.

Gaines, A. M., 1980, Dolomitization kinetics: recent experimental studies. *In* Zenger, D. H., Dunham, J. B., and Ethington, R. L. (eds.), Concepts and Models of Dolomitization. Society of Economic Paleontologists and Mineralogists Spec. Pub. #28, p. 81-85.

Gebelein, C. D., Steinen, R. P., Garrett, P., Hoffman, E. J., Queen, J. M., and Plummer, L. N., 1980, Subsurface dolomitization beneath the tidal flats of central West Andros Island, Bahamas. *In* Zenger, D. H., Dunham, J. B., and Ethington, R. L. (eds.), Concepts and Models of Dolomitization. Society of Economic Paleontologists and Mineralogists Spec. Pub. #28, p. 31-49.

Ghassemi, F., Jakeman, A. J., and Jacobson, G., 1990, Mathematical modelling of sea water intrusion, Nauru Island. Hydrological Processes, v. 4, p. 269-281.

Ghassemi, F., Chen, T. H., Jakeman, A. J., and Jacobson, G., 1993, Two and three-dimensional simulation of seawater intrusion: performances of the "SUTRA" and "HST3D" models. ASGO Journal of Australian Geology and Geophysics, v. 14, no. 2/3, p. 219-226.

Goodell, H. G. and Garman, R. K., 1969, Carbonate geochemistry of Superior Deep Test Well, Andros Island, Bahamas. American Association of Petroleum Geologists Bulletin, v. 53, no. 3, p. 513-536.

Griggs, J. E., and Peterson, F. L., 1993, Ground-water flow dynamics and development strategies at the atoll scale. Ground Water, v. 31, no. 2, p. 209-220.

Hardie, L. A., 1977, Sedimentation on the Modern Carbonate Tidal Flats on Northwest Andros Island, Bahamas. Johns Hopkins University Press, Baltimore, MD, 202 p.

Hardie, L. A., 1987, Perspectives--dolomitization: a critical view of some current views. Journal of Sedimentary Petrology, v. 57, no. 1, p. 166-183.

Illing, L. V., Wells, A. J., and Taylor, J. C. M., 1965, Penecontempory dolomite in the Persian Gulf. *In* Pray, L. C. and Murray, R. C. (eds.), Dolomitization and Limestone Diagenesis. Society of Economic Paleontologists and Mineralogists Spec. Pub. #13, p. 89-111.

Kaufman, J., 1994, Numerical models of fluid flow in carbonate platforms: implications for dolomitization. Journal of Sedimentary Research, v. A64, no. 1, p.128-139.

Kipp, K. L., 1987, HST3D: a computer code for simulation of heat and solute transport in three dimensional ground-water flow systems. US Geological Survey. Water Resources Investigations, Report 86-4095, 517 p.

Knauss, J. A., 1978, Introduction to Physical Oceanography. Prentice Hall, Englewood Cliffs, NJ, 338 p.

Kohout, F. A., 1967, Ground-water flow and the geothermal regime of the Floridian Plateau. Gulf Coast Association of Geological Societies, Transactions, v. 17, p. 339-354.

Kunze, A. W. G., and Quick, T. J., 1994, Tidal water level fluctuations in water wells on San Salvador Island, Bahamas. Bulletin of the Association of Engineering Geologists, v. 31, no. 1, p. 75-89.

Land, L. S., 1983, Dolomitization. American Association of Petroleum Geologists Education Course Note Series, #24, 20 p.

Machel, H. G., and Mountjoy, E. W., 1987, General constraints on extensive pervasive dolomitization--and their application to the Devonian carbonates of western Canada. Bulletin of Canadian Petroleum Geology, v. 35, no. 2, p. 143-158.

McCullough, M. L., and Land, L. S., 1992, Dynamic hydrology and diagenesis of a submerged Pleistocene fringing reef, Discovery Bay, Jamaica. Marine Geology, v. 104, p. 139-151.

McKenzie, J. A., Hsu, K. J., and Schneider, J. F., 1980, Movement of subsurface waters under the sabkha, Abu Dhabi, Uae, and its relation to evaporative dolomite genesis. *In* Zenger, D. H., Dunham, J. B., and Ethington, R. L. (eds.), Concepts and Models of Dolomitization. Society of Economic Paleontologists and Mineralogists Spec. Pub. #28, p. 11-30.

Mottana, A., Crespi, R., and Liborio, G., 1978, Simon and Schuster's Guide to Rocks and Minerals. Simon and Schuster Inc., New York, NY, 607 p.

Mullins, H. T., and Lynts, G. W., 1977, Origin of the northwestern Bahama Platform: review and reinterpretation. Geological Society of America Bulletin, v. 88, p. 1447-1461.

Plummer, L. N., 1975, Mixing of sea water with calcium carbonate ground water. Geological Society of America Mem. 142, p. 219-238.

Reilly, T. E., and Goodman, A. S., 1985, Quantitative analysis of saltwater--freshwater relationships in groundwater systems--a historical perspective. Journal of Hydrology, v. 80, p. 125-160.

Simms, M., 1984, Dolomitization by groundwater-flow systems in carbonate platforms. Gulf Coast Association of Geological Societies, Transactions, v. 34, p. 411-420.

Spencer, M., 1967, Bahamas Deep Test. American Association of Petroleum Geologists Bulletin, v. 51, p. 263-268.

Stoessell, R. K., Ward, W. C., Ford, B. H., and Schuffert, J. D., 1989, Water chemistry and CaCO3 dissolution in the saline part of an open-flow mixing zone, coastal Yucatan Peninsula, Mexico. Geological Society of America Bulletin, v. 101, p. 159-169.

Stumm, W. and Morgan, J. J., 1981, Aquatic Chemistry: An Introduction Emphasizing Chemical Equilibria in Natural Waters, 2nd ed. John Wiley and Sons, New York, NY. 780 p.

Voss, C. I., 1984, SUTRA, Saturated-Unsaturated TRAnsport: a finite-element simulation model for saturated-unsaturated fluid-density-dependent groundwater flow with energy transport or chemically-reactive single-species solute transport. US Geological Survey. Water Resources Investigations, Report 84-4369, 409 p.

Voss, C. I., and Souza, W. R., 1987, Variable density flow and solute transport simulation of regional aquifers containing a narrow freshwater-saltwater transition zone. Water Resources Research, v. 21, no. 10, p. 1851-1866.

Ward, W. C. and Halley, R. B., 1985, Dolomitization in a mixing zone of near-seawater composition, Late Pleistocene, northeastern Yucatan Peninsula. Journal of Sedimentary Petrology, v. 55, p. 407-420.

Weast, R. C., Astle, M. J., and Beyer, W. H., 1986, CRC Handbook of Chemistry and Physics, 67th ed. CRC Press, Inc., Boca Raton, FL.

Weyl, P. K., 1960, Porosity through dolomitization: conservation of mass requirements. Journal of Sedimentary Petrology, v. 30, no. 1, p. 85-90.

Whitaker, F. F., and Smart, P. L., 1993, Circulation of saline ground waters in carbonate platforms: a review and case study from the Bahamas. *In* Horbury, A. D., and Robinson, A. G. (eds.), Diagenesis and Basin Development. American Association of Petroleum Geologists Studies in Geology #36, p. 113-132.

Appendix A

FORTRAN Codes

```
      program velo
C     This program reads the velocity output files from
C     HST3D and writes various output files which
C     can then be imported into SURFER.
C
C
      dimension xcord(32), ycord(2), zcord(70), velox(32,2,70),
     &       veloy(32,2,70), veloz(32,2,70)
      open (unit=10,file='vel.baa',status='old')
      open (unit=11,file='veloc.dat',status='new')
      data xcord /0.,5000.,10000.,15000.,20000.,25000.,30000.,35000.,
     & 40000.,45000.,50000.,55000.,60000.,65000.,70000.,75000.,80000.,
     & 85000.,90000.,95000.,100000.,105000.,110000.,115000.,120000.,
     & 125000.,130000.,135000.,140000.,145000.,150000.,155000./
      data ycord /0.,5./
      data zcord /-3000.,-2950.,-2900.,-2850.,-2800.,-2750.,-2700.,
     & -2650.,-2600.,-2550.,-2500.,-2450.,-2400.,-2350.,-2300.,-2250.,
     & -2200.,-2150.,-2100.,-2050.,-2000.,-1950.,-1900.,-1850.,-1800.,
     & -1750.,-1700.,-1650.,-1600.,-1550.,-1500.,-1450.,-1400.,-1350.,
     & -1300.,-1250.,-1200.,-1150.,-1100.,-1050.,-1000.,-950.,-900.,
     & -850.,-800.,-750.,-700.,-650.,-600.,-550.,-500.,-450.,-400.,
     & -350.,-300.,-250.,-210.,-175.,-140.,-110.,-85.,-65.,-49.,-36.,
     & -27.,-20.,-15.,-10.,-5.,0./
      nx=32
      ny=2
      nz=70
C
C*****************************
C Read in the velocity data
C
      read (10,98)
      do 50 j=1,ny
        do 40 k=nz,1,-1
          read (10,99) (velox(i,j,k), i=1,10)
C          write (11,*) i,j,k,velox(1,j,k)
   40   continue
        read(10,198)
        do 10 k=nz,1,-1
          read (10,99) (velox(i,j,k), i=11,20)
   10   continue
        read (10,198)
        do 11 k=nz,1,-1
          read (10,99) (velox(i,j,k), i=21,30)
   11   continue
        read (10,198)
        do 12 k=nz,1,-1
          read (10,99) (velox(i,j,k), i=31,31)
   12   continue
        read (10,198)
   50 continue
```

```
C
      read (10,298)
      do 51 j=1,ny-1
        do 41 k=nz,1,-1
          read (10,99) (veloy(i,j,k), i=1,10)
C          write (11,*) i,j,k,veloy(1,j,k)
   41   continue
        read (10,198)
        do 30 k=nz,1,-1
          read (10,99) (veloy(i,j,k), i=11,20)
   30   continue
        read (10,198)
        do 31 k=nz,1,-1
          read (10,99) (veloy(i,j,k), i=21,30)
   31   continue
        read (10,198)
        do 32 k=nz,1,-1
          read (10,99) (veloy(i,j,k), i=31,32)
   32   continue
        read (10,198)
   51 continue
C
      read (10,298)
      do 52 j=1,ny
        do 42 k=nz-1,1,-1
          read (10,99) (veloz(i,j,k), i=1,10)
C          write (11,*) i,j,k,veloz(1,j,k)
   42   continue
        read (10,198)
        do 60 k=nz-1,1,-1
          read (10,99) (veloz(i,j,k), i=11,20)
   60   continue
        read (10,198)
        do 61 k=nz-1,1,-1
          read (10,99) (veloz(i,j,k), i=21,30)
   61   continue
        read (10,198)
        do 62 k=nz-1,1,-1
          read (10,99) (veloz(i,j,k), i=31,32)
   62   continue
        read (10,198)
   52 continue
C
C
C*****************************
C
C
C*****************************
C    output of x, z, velocity and angle
       write (*,*) 'Which slice? '
```

```
      read *, islice
      j=islice
        do 470 k=1,nz-1
          do 480 i=1,nx-1
            if (abs(velox(i,j,k)).gt.1.00e-30) then
              go to 479
            elseif ((abs(velox(i,j,k)).lt.1.00e-30).and.
     &       (veloz(i,j,k).lt.0)) then
              write (11,199) xcord(i)+(xcord(i+1)-xcord(i))/2,
     &         zcord(k)+(zcord(k+1)-zcord(k))/2,abs(veloz(i,j,k)),
     &         -90.
              go to 480
            elseif ((abs(velox(i,j,k)).lt.1.00e-30).and.
     &       (veloz(i,j,k).gt.0)) then
              write (11,199) xcord(i)+(xcord(i+1)-xcord(i))/2,
     &         zcord(k)+(zcord(k+1)-zcord(k))/2,veloz(i,j,k),
     &         90.
               go to 480
            else
            write (*,*) 'ack!',velox(i,j,k),veloz(i,j,k)
            go to 480
            end if
C            mult. veloz by 20x to account for vertical exag.?
C            veloz(i,j,k)=veloz(i,j,k)*20
  479       veloc=sqrt((velox(i,j,k)*velox(i,j,k))+(veloz(i,j,k)*
     &          veloz(i,j,k)))
            veloz(i,j,k)=veloz(i,j,k)*20
              if (velox(i,j,k).lt.0) then
              angle=180-((atan(veloz(i,j,k)/abs(velox(i,j,k))))
     &          *(57.296))
              go to 481
              end if
            angle=(atan(veloz(i,j,k)/abs(velox(i,j,k))))*(57.296)
            go to 481
  481       write (11,199) xcord(i)+(xcord(i+1)-xcord(i))/2,
     &        zcord(k)+(zcord(k+1)-zcord(k))/2,veloc,angle
  480     continue
  470   continue
C
   98 format (///////////////)
   99 format (5x,10e13.7)
  198 format (///)
  199 format (2f10.2,e12.4,f10.2)
  299 format (f8.2,i5)
  298 format (/////)
  599 format (3f10.2,3e12.4)
  699 format (2f10.2,e12.4)
  799 format (3f10.2,e12.4)
      stop
      end
```

```
      program rdinput
C      This should work, without these lines anyway...
C      BE SURE TO CHECK FORMATS AND MAKE SURE EVERYTHING IS READ IN PROPERLY.
C     This program reads the pressure output file from
C     HST3D and writes an output file which contains pressures
C     in a format that can be read into the HST3D input file for
C     boundary or initial conditions
C
C
      dimension xcord(32), ycord(2), zcord(70), var(32,2,70)
      open (unit=10,file='pres.baa',status='old')
      open (unit=11,file='pres.ipt',status='new')
      data xcord /0.,5000.,10000.,15000.,20000.,25000.,30000.,35000.,
     & 40000.,45000.,50000.,55000.,60000.,65000.,70000.,75000.,80000.,
     & 85000.,90000.,95000.,100000.,105000.,110000.,115000.,120000.,
     & 125000.,130000.,135000.,140000.,145000.,150000.,155000./
      data ycord /0.,5./
      data zcord /-3000.,-2950.,-2900.,-2850.,-2800.,-2750.,-2700.,
     & -2650.,-2600.,-2550.,-2500.,-2450.,-2400.,-2350.,-2300.,-2250.,
     & -2200.,-2150.,-2100.,-2050.,-2000.,-1950.,-1900.,-1850.,-1800.,
     & -1750.,-1700.,-1650.,-1600.,-1550.,-1500.,-1450.,-1400.,-1350.,
     & -1300.,-1250.,-1200.,-1150.,-1100.,-1050.,-1000.,-950.,-900.,
     & -850.,-800.,-750.,-700.,-650.,-600.,-550.,-500.,-450.,-400.,
     & -350.,-300.,-250.,-210.,-175.,-140.,-110.,-85.,-65.,-49.,-36.,
     & -27.,-20.,-15.,-10.,-5.,0./
      nx=32
      ny=2
      nz=70
      read (10,98)
      do 50 j=1,ny
        do 40 k=nz,1,-1
          read (10,99) (var(i,j,k), i=1,10)
          write (*,*) i,j,k
   40   continue
        read(10,198)
        do 30 k=nz,1,-1
          read (10,99) (var(i,j,k), i=11,20)
   30   continue
        read (10,198)
        do 25 k=nz,1,-1
          read (10,99) (var(i,j,k), i=21,30)
   25   continue
        read (10,198)
        do 26 k=nz,1,-1
          read (10,99) (var(i,j,k), i=31,32)
   26   continue
        read (10,198)
   50 continue
C
```

```
      do 70 k=1,nz
        do 80 j=1,ny
          write (11,199)(var(i,j,k), i=1,nx)
 80     continue
 70   continue
 98 format (/////////////////)
 99 format (5x,11g13.7)
198 format (///)
199 format (6g13.7)
299 format (g9.4,i5)
    stop
    end
```

```
      program pres2d
C     This program reads the pressure/head output file from
C     HST3D and writes an output file which contains x, z and
C     pressure/head.  This file can then be imported into SURFER.
C     (Also to be used for solute concentrations.)
C
C
      dimension xcord(32), ycord(2), zcord(70), var(32,2,70)
      open (unit=10,file='pres.baa',status='old')
      open (unit=11,file='pres.dat',status='new')
      data xcord /0.,5000.,10000.,15000.,20000.,25000.,30000.,35000.,
     & 40000.,45000.,50000.,55000.,60000.,65000.,70000.,75000.,80000.,
     & 85000.,90000.,95000.,100000.,105000.,110000.,115000.,120000.,
     & 125000.,130000.,135000.,140000.,145000.,150000.,155000./
      data ycord /0.,5./
      data ycord /0.,5./
      data zcord /-3000.,-2950.,-2900.,-2850.,-2800.,-2750.,-2700.,
     & -2650.,-2600.,-2550.,-2500.,-2450.,-2400.,-2350.,-2300.,-2250.,
     & -2200.,-2150.,-2100.,-2050.,-2000.,-1950.,-1900.,-1850.,-1800.,
     & -1750.,-1700.,-1650.,-1600.,-1550.,-1500.,-1450.,-1400.,-1350.,
     & -1300.,-1250.,-1200.,-1150.,-1100.,-1050.,-1000.,-950.,-900.,
     & -850.,-800.,-750.,-700.,-650.,-600.,-550.,-500.,-450.,-400.,
     & -350.,-300.,-250.,-210.,-175.,-140.,-110.,-85.,-65.,-49.,-36.,
     & -27.,-20.,-15.,-10.,-5.,0./
      nx=32
      ny=2
      nz=70
      read (10,98)
      do 50 j=1,ny
        do 40 k=nz,1,-1
          read (10,99) (var(i,j,k), i=1,10)
          write (*,*) i,j,k
40    continue
      read(10,198)
      do 30 k=nz,1,-1
        read (10,99) (var(i,j,k), i=11,20)
30    continue
      read (10,198)
      do 25 k=nz,1,-1
        read (10,99) (var(i,j,k), i=21,30)
25    continue
      read (10,198)
      do 26 k=nz,1,-1
        read (10,99) (var(i,j,k), i=31,32)
26    continue
      read (10,198)
50  continue
C
```

```
      write (*,*) 'Which Slice?'
      read *, slice
      j=slice
        do 70 k=1,nz
          do 80 i=1,nx
            write (11,199) xcord(i),zcord(k),var(i,j,k)
 80       continue
 70     continue
 98   format (////////////////)
 99   format (5x,11g13.7)
198   format (///)
199   format (3g13.7)
299   format (g9.4,i5)
      stop
      end
```

```
      program balance
C     This program reads the fluid/heat/solute balance output file
C     from HST3D and writes an output file containing the rate of
C     change of fluid OR heat OR solute at each timestep.  This
C     data can be used to graphically represent the model reaching
C     a steady state solution.
C
C
      character*13 time,value
      character*8 fred
      open (unit=10,file='bal.in',status='old')
      open (unit=11,file='bal.dat',status='new')
      write (*,*) 'fluid, heat, or solute balance?'
      read (*,'(A8)') fred
      write (*,*) 'simulation length?'
      read *, timchg
      write (*,*) 'timestep printout interval?'
      read *, deltim
      nt=timchg/deltim
      if (fred.eq.'heat') then
      go to 40
      end if
      if (fred.eq.'solute') then
      go to 40
      end if
C
      do 30 j=1,nt
        read (10,196) time
        read (10,197) value
        write (11,198) value,time
        read (10,199)
   30 continue
        go to 195
   40 do 41 j=1,nt
        read (10,296) time
        read (10,297) value
        write (11,198) value,time
        read (10,299)
   41 continue
  195 continue
  196 format (///////,86x,A13)
  197 format (//////,62x,A13)
  198 format (2A13)
  199 format (////////////////////////////////////////////////////)
  296 format (///////,86x,A13)
  297 format (////////////,62x,A13)
  299 format (////////////////////////////////////////////////)
      stop
      end
```

```
      program SGIgraph
C     This program reads the temperature output file from
C     HST3D and writes an output file which contains xy or xz and
C     temperature.  This file can then be imported into SURFER.
C
C
      dimension xcord(32), ycord(2), zcord(70), var(32,2,70)
      open (unit=10,file='art.in',status='old')
      open (unit=11,file='art.dat',status='new')
      data xcord /0.,5000.,10000.,15000.,20000.,25000.,30000.,35000.,
     & 40000.,45000.,50000.,55000.,60000.,65000.,70000.,75000.,80000.,
     & 85000.,90000.,95000.,100000.,105000.,110000.,115000.,120000.,
     & 125000.,130000.,135000.,140000.,145000.,150000.,155000./
      data ycord /0.,5./
      data zcord /-3000.,-2950.,-2900.,-2850.,-2800.,-2750.,-2700.,
     & -2650.,-2600.,-2550.,-2500.,-2450.,-2400.,-2350.,-2300.,-2250.,
     & -2200.,-2150.,-2100.,-2050.,-2000.,-1950.,-1900.,-1850.,-1800.,
     & -1750.,-1700.,-1650.,-1600.,-1550.,-1500.,-1450.,-1400.,-1350.,
     & -1300.,-1250.,-1200.,-1150.,-1100.,-1050.,-1000.,-950.,-900.,
     & -850.,-800.,-750.,-700.,-650.,-600.,-550.,-500.,-450.,-400.,
     & -350.,-300.,-250.,-210.,-175.,-140.,-110.,-85.,-65.,-49.,-36.,
     & -27.,-20.,-15.,-10.,-5.,0./
      nx=32
      ny=2
      nz=70
      read (10,98)
      do 50 j=1,ny
        do 40 k=nz,1,-1
          read (10,99) (var(i,j,k), i=1,10)
          write (*,*) i,j,k
   40   continue
        read(10,198)
        do 30 k=nz,1,-1
          read (10,99) (var(i,j,k), i=11,20)
   30   continue
        read (10,198)
        do 25 k=nz,1,-1
          read (10,99) (var(i,j,k), i=21,30)
   25   continue
        read (10,198)
        do 26 k=nz,1,-1
          read (10,99) (var(i,j,k), i=31,32)
   26   continue
        read (10,198)
   50 continue
C
```

```
      write (*,*) 'Which Slice?'
      read *, slice
      j=slice
        do 70 k=1,nz
          do 80 i=1,nx
            write (11,199) xcord(i),zcord(k),1.,var(i,j,k)
 80       continue
 70     continue
 98   format (/////////////////)
 99   format (5x,11g13.7)
198   format (///)
199   format (4g11.4)
299   format (g9.4,i5)
      stop
      end
```

```
      program bibble
C     This program reads the velocity output file generated by
C     PROGRAM VELO and writes an output file containing maximum,
C     minimum and average velocities (magnitudes ONLY).
C
C
      dimension veloc (2000)
      open (unit=10,file='veloc.dat',status='old')
      open (unit=11,file='range.dat',status='new')
      write (*,*) 'number of lines in input file?'
      read *, nt
C
      do 30 j=1,nt
        read (10,98) vel
        if (vel.lt.0) vel=abs(vel)
        veloc(j)=vel
C        write (*,*) veloc(j)
   30 continue
C
      velmin=10000
      velmax=0
      do 40 j=1,nt
        if (velmin.gt.veloc(j)) velmin=veloc(j)
   40 continue
      do 50 j=1,nt
        if (velmax.lt.veloc(j)) velmax=veloc(j)
   50 continue
C
      totvel=veloc(1)
      do 60 j=2,nt
        totvel=totvel+veloc(j)
C        write (*,*) totvel
   60 continue
      avgvel=totvel/nt
      write (11,198) velmin,velmax,avgvel
C
   98 format (20x,e13.5)
  198 format (3e13.5)
      stop
      end
```

APPROVED: Jean M. Baker

DATE: August 31, 1994